

Structure-dependent QED in $B^- \rightarrow \ell^- \bar{\nu}(\gamma)$

Matthew Rowe,¹ Roman Zwicky¹

¹*Higgs Centre for Theoretical Physics, School of Physics and Astronomy, University of Edinburgh, Edinburgh, EH9 3JZ, Scotland*

E-mail: m.j.rowe@sms.ed.ac.uk, roman.zwicky@ed.ac.uk

ABSTRACT: Based on explicitly gauge invariant interpolating operators we compute complete next-leading order QED-corrections for leptonic decays. These are sizeable since the helicity-suppression in V-A interactions allows for structure-dependent collinear logs. We have explicitly checked that these logs are absent for helicity-unsuppressed Yukawa-type transitions. Based on $B \rightarrow \gamma$ form factors we present the rates for $B^- \rightarrow (\mu^-, \tau^-) \bar{\nu}(\gamma)$ in differential and integrated form as a function of the photon energy cut-off E_γ^{cut} . The effect of the virtual structure-dependent corrections are approximately +5% and +3% for the μ - and τ -channel respectively. The structure dependence of the real radiation exceeds that of the virtual one for $E_\gamma^{\text{cut}}|_\mu > 0.18(3)$ GeV and is subdominant for the tau channel even when fully inclusive.

Contents

1	Introduction	1
2	The gauge invariant formalism for $B^- \rightarrow \ell^- \bar{\nu}(\gamma)$	2
2.1	The main process	3
2.2	The LSZ-factor	5
3	The computation	6
3.1	Leading order	7
3.2	Virtual corrections	8
3.2.1	Infrared sensitive (soft) terms	9
3.2.2	Gauge invariance	11
3.2.3	Renormalisation	11
3.2.4	Final virtual rate	12
3.3	Real radiation	13
3.3.1	The amplitude	13
3.3.2	Final radiative rate	14
4	Collinear logs	15
4.1	Universal IR logs from the splitting function	15
4.2	The virtual contribution	16
4.3	The real radiation	18
5	Numerics and phenomenology	19
5.1	Sum rule numerics	19
5.2	Outlook on phenomenology	22
6	Conclusions and summary	24
A	Conventions, inputs and plots	25
A.1	Condensate contributions	25
A.2	More detailed plots	28
B	Further aspects	29
B.1	On the necessity of all cuts	29
B.2	Toy model	31

1 Introduction

It has been known for a long time that QED challenges the notion of a charged elementary particle because of the emission of infinitely many soft photons leading to seemingly infrared (IR) divergent processes. At the conceptual level this problem has been resolved by abandoning the one-particle Fock space in favour of the coherent state formalism [1–5]. A more pragmatic solution is the well-known Bloch-Nordsieck cancellation mechanism [6], whereby virtual corrections and real emissions processes are added consistently at each order in the fine structure constant $\alpha \equiv e^2/(4\pi) \approx 1/137$ giving rise to IR-finite processes. As experiment is seldom fully inclusive the photon-energy is either cut-off explicitly or one considers the photon-energy differential rate. This leads to large soft-logs but since they originate from the soft region the structure of the particles is not resolved and thus treating the latter in the point-like approximation (i.e. scalar QED) suffices and is well-understood including resummation [7, 8]. The other sizeable logs are the collinear ones which arise when the photon is collinear to a light charged particle, such as an electron in a B -decay. For example, in $B \rightarrow Ke^+e^-$ collinear logs of the type $\frac{\alpha}{\pi} \ln(m_e/m_B)$ lead to corrections of up to 10-20% depending on the phase space region [9, 10]. Since the collinearity does not restrain the photon energy the point-like approximation is not applicable and structure-dependence can give rise to large (hard)-collinear logs. However, using gauge invariance and the KLN-theorem [11, 12], which extends the Bloch-Nordsieck idea to massless charged particles, it was shown that no such logs can arise [9]. There are though exceptions: i) when the collinear charged particle is composite e.g. π^- or ii) when the KLN-theorem does not need to hold. It is precisely the second exception that applies to $B^- \rightarrow \ell^- \bar{\nu}$ -type decays mediated by V-A interaction as in the Standard Model (SM). The point is that the amplitude is chirally suppressed $\mathcal{A} \propto m_\ell \ln m_\ell$ and thus finite for $m_\ell \rightarrow 0$ and therefore blind to the KLN-theorem which is based on unitarity cancelling IR divergences [13, 14].

To resolve hadrons one then needs a non-perturbative formalism. Possibly the most natural setting is chiral perturbation theory (ChPT) as it extends the point-like approximations through its energy expansion (e.g. [15–18] and [19–21] for leptonic and semi-leptonic decays respectively). However it does not apply to heavy decays and the other methods such as lattice QCD face, one way or another, the challenge that the standard interpolating operator for a B_q -meson

$$J_B = m_+ \bar{b}i\gamma_5 q, \quad m_\pm = m_b \pm m_q, \quad \langle B^- | J_B | 0 \rangle = m_B^2 f_B, \quad (1.1)$$

is not QED gauge invariant for a charged B_q -meson. In the context of QCD sum rules a solution was proposed [14] by introducing a long distance (on-shell) B -meson in terms of a scalar field Φ_B for which the generalised LSZ-factor has been shown to be IR-finite. In this paper we explicitly verify that all the universal collinear and soft logs are reproduced separately for the virtual and the real rates thereby validating the approach. On the lattice the interpolating operator problem disappears in the limit of infinite Euclidean time separation of the meson source as the exact LSZ formula emerges [22–24].¹ Numerical

¹In addition there is an explicit gauge invariant formulation using so-called C^* -boundary conditions [25].

QED studies include virtual effects in $(\pi, K) \rightarrow \ell \bar{\nu}$ [26], including real radiation [27], real radiation in $D_s \rightarrow \ell \bar{\nu}$ decays [28, 29] and now very recently for $B_s \rightarrow \mu^+ \mu^- (\gamma)$ [30]. QED effects have also been investigated in soft-collinear effective theory (SCET) [31, 32] and specifically for $B^- \rightarrow \ell^- \bar{\nu}$ [33] where the interpolating operator problem is replaced by defining process-dependent light-cone distribution amplitudes [34, 35].

In experiment QED-corrections are dealt with by using Monte-Carlo generators such as PHOTOS [36–39], or the PHOTONS++ module [40] of SHERPA [41] for which $B^- \rightarrow \ell^- \bar{\nu}$ structure-dependent corrections have not yet been implemented since they are unknown.² In this paper we close this gap by computing the virtual structure-dependent corrections for $B^- \rightarrow \ell^- \bar{\nu}$, applying the above mentioned framework [14]. The structure-dependent part of the real radiation is described by the two $B \rightarrow \gamma$ form factors computed in sum rules on the light-cone at NLO in α_s [42].³ Including structure-dependent virtual and real contributions from different sources is not a problem since they are separately IR-finite (unlike scalar QED). The numerical effects relative to scalar QED, which is sizeable by itself, are found to be relevant with respect to other inputs such as the B -meson decay constant and $|V_{ub}|$ (cf. Sec. 5.2). While we provide corrections for the $B^- \rightarrow \ell^- \bar{\nu} (\gamma)$, our framework extends to D - and possibly K -mesons. Neutral decays modes such as $B_s \rightarrow \mu^+ \mu^-$ are simpler as then the long-distance field Φ_B is not required but the kinematics require a slightly different computation.

The paper is organised as follows. In Sec. 2 the conceptual framework is summarised, followed by the computation in Sec. 3 and the discussion of the collinear logs in Sec. 4. Numerical results including comparison to the literature are presented in Sec. 5. The paper ends with conclusions and a summary in Sec. 6. Appendices contain for example the computational results of the condensates, a discussion on the necessity of all cuts and further plots.

2 The gauge invariant formalism for $B^- \rightarrow \ell^- \bar{\nu} (\gamma)$

As stated in the introduction the key change is the introduction of a long-distance B -meson Φ_B to render the interpolating current (1.1) gauge invariant [14]

$$\mathcal{J}_B \equiv J_B \Phi_B, \quad \mathcal{Z}_B \equiv \langle B^- | \mathcal{J}_B | \Phi_{B^-} \rangle. \quad (2.1)$$

We drop the “(0)” superscript with respect to the above-mentioned reference. It is useful to define the charge assignments to the currents

$$Q_{\mathcal{J}_B} \equiv Q_\Phi + Q_q - Q_b, \quad Q_{\mathcal{Z}_B} \equiv Q_q - Q_b. \quad (2.2)$$

The matrix element \mathcal{Z}_B takes on the rôle of the LSZ-factor and has been shown to be IR-finite and (explicitly) gauge invariant [14]. Its key elements will be discussed further

²Hence current Monte-Carlo QED-effects are based on scalar QED (point-like approximation).

³Whereas the standard application of these form factors are to describe the phenomenology of $\bar{B}^- \rightarrow \ell^- \bar{\nu} \gamma$ [43–52] or $B_{d,s} \rightarrow \ell^+ \ell^- \gamma$ [53–56, 56, 57, 57–59] decays, they equally serve as real radiation in the soft region for $\bar{B}^- \rightarrow \ell^- \bar{\nu}$ and $B_{d,s} \rightarrow \ell^+ \ell^-$ respectively.

below. The decay rate, with the Bloch-Nordsieck cancellation mechanism in place is given by

$$\Gamma(B^- \rightarrow \ell^- \bar{\nu}(\gamma)) = \frac{1}{|\mathcal{Z}_B|^2} \times \int_{E_\gamma^{\text{cut}}} d\Phi_\gamma |\mathcal{Z}_B|^2 (|\mathcal{A}(B^- \rightarrow \ell^- \bar{\nu})|^2 \delta(\Phi_\gamma) + |\mathcal{A}(B^- \rightarrow \ell^- \bar{\nu} \gamma)|^2) , \quad (2.3)$$

where $E_\gamma^{\text{cut}} > E_\gamma$ is the photon energy cut-off, in the rest frame of the decaying particle. The delta function $\delta(\Phi_\gamma)$ in the photon kinematic variables, to be made more precise further below, singles out the virtual contribution. The point of the sum rule procedure is that both the LSZ-factor $|\mathcal{Z}_B|^2$ and the integrand are computed separately from appropriate correlation functions as outlined below.

2.1 The main process

The integrand in (2.3), can be extracted from the following correlation function

$$\begin{aligned} \Pi^{(\gamma)}(p_B^2, p_\Phi^2) &= i \int_x e^{ixr} \langle \ell \bar{\nu}(\gamma) | T \mathcal{J}_B(x) (-i \mathcal{L}_W(0)) | \Phi_B(p_\Phi) \rangle \\ &= \int \frac{ds}{2\pi i} \frac{\text{disc}_s[\Pi^{(\gamma)}(s, p_\Phi^2)]}{s - p_B^2 - i0} = \frac{\mathcal{Z}_B i \mathcal{A}(B^- \rightarrow \ell^- \bar{\nu}(\gamma))}{m_B^2 - p_B^2} + \dots , \end{aligned} \quad (2.4)$$

which we have written as a dispersion relation of which the residuum of the lowest lying state carries the information of interest. The dots denote higher states in the spectrum which will be suppressed by the usual Borel transform. Above $\int_x \equiv \int d^d x$ is a shorthand used hereafter, $\mathcal{A}^{(\gamma)} \equiv \langle \ell \bar{\nu}(\gamma) | -\mathcal{L}_W | B^- \rangle$ the amplitude and \mathcal{L}_W the electroweak Lagrangian

$$\mathcal{L}_W = -g_{\text{eff}} \bar{\ell} \Gamma^\mu \nu \bar{u} \hat{\Gamma}_\mu b , \quad \Gamma_\mu = \gamma_\mu (C_V + C_A \gamma_5) , \quad \hat{\Gamma}_\mu = \gamma_\mu (1 - \gamma_5) , \quad (2.5)$$

with $C_{V(A)} = 1(-1)$ in the SM

$$p_\Phi = p_B + r , \quad q = p_B - k , \quad g_{\text{eff}} = -\frac{G_F}{\sqrt{2}} V_{\text{ub}} , \quad (2.6)$$

with G_F the Fermi constant and V_{ub} the CKM matrix element governing the $b \rightarrow u$ transition. The momenta r is auxiliary as it is used to distinguish between the on-shell p_Φ and the off-shell p_B momenta used for the dispersion relation. We comment on its role and how it finally does not play a role further below. The $b\bar{u}$ -flavour is chosen for concreteness and replacement by other flavour structures is straightforward. It is important to distinguish p_Φ in the real and virtual case

$$p_\Phi|_{\text{virt}} = l_1 + l_2 , \quad p_\Phi|_{\text{real}} = l_1 + l_2 + k , \quad (2.7)$$

where $l_{1,2}$ and k are lepton and photon momenta respectively.

Theoretical considerations: If the meson that J_B interpolates was stable and we were able to apply a perfect LSZ projection then there would be no need to be concerned with gauge dependence as it would simply cancel in the ratio (2.3). In other words all artefacts are contained in $|\mathcal{Z}_B|$. The problem is that a perfect LSZ can never be achieved in practice for a composite particle in a non-trivial theory and thus the necessity to act. Concretely, in QCD sum rules J_B is not perfectly on-shell since the dispersive integral is approximated by a perturbative computation. This is where $\Phi_B(p_\Phi)$ comes in as it is on-shell and the auxiliary momenta r in (2.6) parameterises that. In order to recover the correct soft logs one must ensure [14]

$$p_\Phi^2 = m_B^2, \quad (2.8)$$

which intuitively seems the most natural choice in any case.

Let us turn to why it is interesting to consider, besides the V-A interaction, the S-P interaction of Yukawa-type. As previously stated, the reason there are structure-dependent logs in the V-A case is that the amplitude is chirally suppressed. This suppression is lifted in the S-P case. Symbolically we have

$$\begin{aligned} \mathcal{A}(B \rightarrow \ell \bar{\nu})|_{\text{V-A}} &\propto \mathcal{O}(m_\ell) + \mathcal{O}(\alpha) m_\ell \ln m_\ell, \\ \mathcal{A}(B \rightarrow \ell \bar{\nu})|_{\text{S-P}} &\propto \mathcal{O}(m_\ell^0) + \mathcal{O}(\alpha) m_\ell^0 \ln m_\ell, \end{aligned} \quad (2.9)$$

abbreviating $B^- \rightarrow \ell^- \bar{\nu}$ to $B \rightarrow \ell \bar{\nu}$ here and occasionally elsewhere. Hence the S-P can serve as a test case to reproduce the hard-collinear logs as done and advertised in [13]. The hard-collinear logs can be reproduced using the splitting function. Formally the S-P case simply follows through substitution $\gamma_\mu \rightarrow \mathbb{1}$ for $\hat{\Gamma}_\mu$ and Γ_μ in (2.5). Note that for the real radiation the helicity-suppression is lifted for the V-A interactions. Hence, for the SM case there are then two effects due to the helicity-suppression:

- i) large hard-collinear logs for the virtual structure-dependent QED-corrections
- ii) significant enhancement of the real radiation for large E_γ^{cut}

Where ii) is well-appreciated point i) is not and its clarification is one of the main points of this paper. These effects are of course more pronounced for the muon since the tau mass is rather large.

The computation: The amplitude times the LSZ-factor, the square root of the integrand, is then obtained by the usual sum rule procedure

$$i\mathcal{A}(B^- \rightarrow \ell^- \bar{\nu}(\gamma)) = \frac{1}{\mathcal{Z}_B} \int_{m_+^2}^{s_0} ds e^{\frac{(m_B^2 - s)}{M^2}} \rho_{\Pi(\gamma)}(s), \quad (2.10)$$

where $2\pi i \rho_{\Pi}(s) = 2i \text{Im} \Pi(s, m_B^2) = \text{disc}_s \Pi(s, m_B^2)$ by analyticity (and the Schwartz reflection principle). In the above M^2 and s_0 are the Borel parameter and continuum threshold which are the sum rule specific parameters. It is convenient to decompose this quantity into LO and NLO in α parts and perturbative versus quark condensate parts

$$\rho_{\Pi(\gamma)}(s) = \rho_{\Pi(\gamma), \mathbb{1}}^{(0)}(s) + \langle \bar{q}q \rangle \rho_{\Pi(\gamma), \bar{q}q}^{(0)}(s) + \frac{\alpha}{\pi} (\rho_{\Pi(\gamma), \mathbb{1}}^{(2)}(s) + \langle \bar{q}q \rangle \rho_{\Pi(\gamma), \bar{q}q}^{(2)}(s)). \quad (2.11)$$

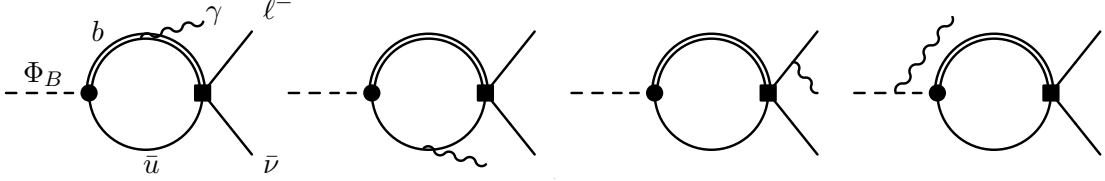


Figure 1: Diagrams contributing to $\Pi^\gamma(p_B^2, p_\Phi^2)$ in (2.4) (i.e. the radiative or real emission part). The last diagram is specific to the Φ_B -particle. The black circle denotes the \mathcal{J}_B operator, while the black square denotes the weak vertex \mathcal{L}_w . We stress that for the real structure dependent part we take external form factors [42] which include many more contributions to the above diagrams. E.g. higher twist in the photon distribution amplitude and $\mathcal{O}(\alpha_s)$.

The quantity ρ_Π is an implicit function of $\{m_B^2, m_b, m_q, m_\ell\}$, as well as the photon energy E_γ and the photon angle c_γ (to be made precise later) in the case of the real emission. The real emission and virtual diagrams are depicted in Fig. 1 and Fig. 2 respectively. It is observed that due to the presence of the (charged) Φ_B the number of diagrams proliferates. As discussed in Sec. 3.3 the calculation for the real radiative rate can essentially be recast in terms of $B \rightarrow \gamma$ form factors which contain all the structure-dependence. We take the light-cone sum rule (LCSR) computation in [42] which is NLO in α_s and itself valid for $q^2 < 14 \text{ GeV}^2$. This computation has been extended to the $B^*(B_1)$ -pole, using the residue from a different (but related computation) [60], with a z -parametrisation ansatz [42]. In fact it is the proximity to the pole of our domain of interest which makes it hard to impossible to compute the form factor directly with perturbative methods.

On the auxiliary momenta r : How does the unphysical momenta r disappear from the final calculation? First, Lorentz structures involving r that appear in the calculation such as $\bar{u}\not{r}v$, $r \cdot \epsilon^*$ etc are considered extra unphysical information and can be discarded. Second, scalar products involving r are $\mathcal{O}(p_B^2 - m_B^2)$ and would vanish in the case of a perfect LSZ. In the sum rule they give rise to small effects since the dispersion integral enforces $p_B^2 \approx m_B^2$ numerically and they will enter the uncertainty budget. Third, the freedom in choosing other scalar products such as r^2 and $l_2 \cdot r$ allows us to set

$$r^2 = 0, \quad l_2 \cdot r = 0. \quad (2.12)$$

The choice $l_2 \cdot r = 0$, simply serves to remove the auxiliary momenta r and is in particular feasible since the neutrino is massless (the scalar product of two lightlike vectors can be set to zero). All of these concepts were tested in a toy model presented in App. B.2. The reader might find it helpful to disentangle the inner workings of this approach within that simplified setting. We stress that in both the toy model and our hadronic framework all universal IR logs have been recovered.

2.2 The LSZ-factor

The LSZ-factor (2.1) can be extracted from the following diagonal correlation function

$$C(p_B^2, p_\Phi^2) = i \int_x e^{ixr} \langle \Phi_B(p_\Phi) | T \mathcal{J}_B(x) \mathcal{J}_B^\dagger(0) | \Phi_B(p_\Phi) \rangle$$

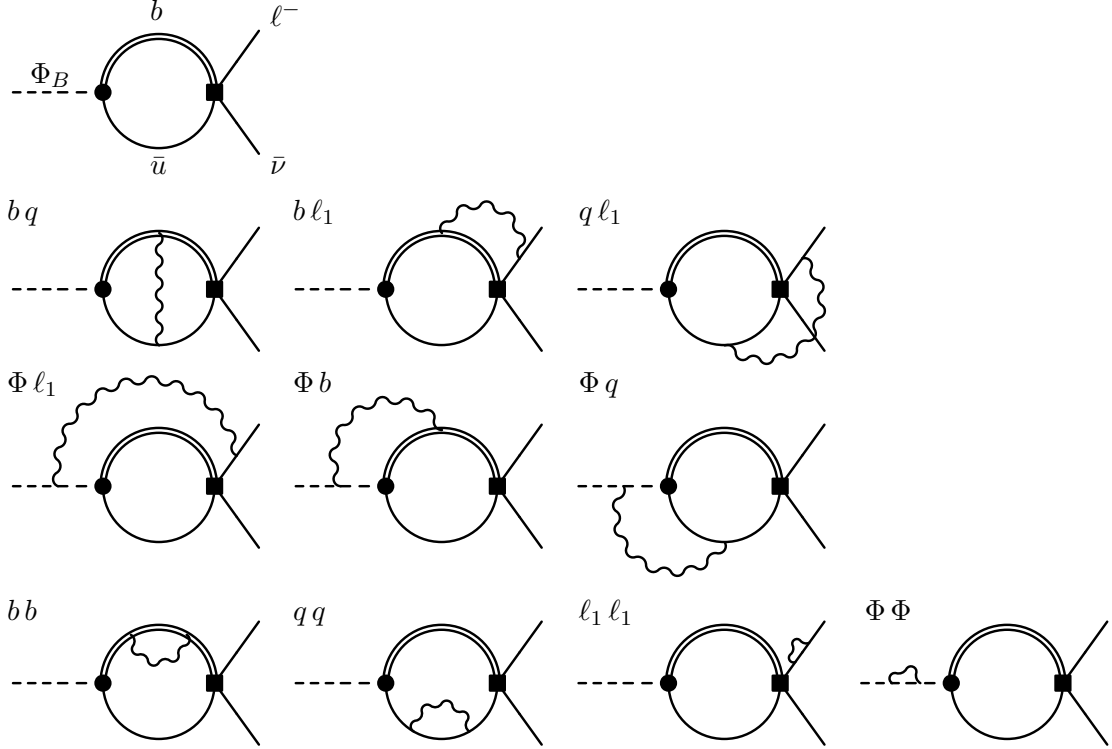


Figure 2: Diagrams contributing to $\Pi(p_B^2, p_\Phi^2)$ in (2.4) (ie. the non-radiative part, hence no (γ) superscript). Top line is the LO diagram and the third line and the last diagram are specific to the Φ_B -particle.

$$= \int \frac{ds}{2\pi i} \frac{\text{disc}_s C(s, m_B^2)}{s - p_B^2 - i0} = \frac{|\mathcal{Z}_B|^2}{m_B^2 - p_B^2} + \dots, \quad (2.13)$$

where (2.8) has been assumed and as before the dots stand for higher states. The LSZ-factor is formally given by $|\mathcal{Z}_B|^2 = \lim_{p_B^2 \rightarrow m_B^2} (m_B^2 - p_B^2) C(p_B^2, m_B^2)$ and translates to

$$|\mathcal{Z}_B|^2 = \int_{m_+^2}^{s_0} ds e^{\frac{(m_B^2 - s)}{M^2}} \rho_C(s), \quad (2.14)$$

for the sum rule procedure. As previously $2\pi i \rho_C(s) = 2i \text{Im} C(s, m_B^2) = \text{disc}_s C(s, m_B^2)$ and M^2 and s_0 are the Borel parameter and continuum threshold. The analogous breakdown of the spectral density reads

$$\rho_C(s) = \rho_{C,1}^{(0)}(s) + \langle \bar{q}q \rangle \rho_{C,\bar{q}q}^{(0)}(s) + \frac{\alpha}{\pi} (\rho_{C,1}^{(2)}(s) + \langle \bar{q}q \rangle \rho_{C,\bar{q}q}^{(2)}(s)), \quad (2.15)$$

and implicitly depends on the further variables $\{m_B^2, m_b, m_q\}$ and the usual renormalisation scale(s). In the QCD limit, when Φ_B is removed, one recovers the standard sum rule for f_B with $|\mathcal{Z}_B|^2 \rightarrow m_B^4 f_B^2$. The corresponding Feynman diagrams are given in Fig. 3.

3 The computation

The computation consists of the leading order (LO), real emission and the virtual contribution. The most labour intensive part is computing the two loop virtual diagrams,

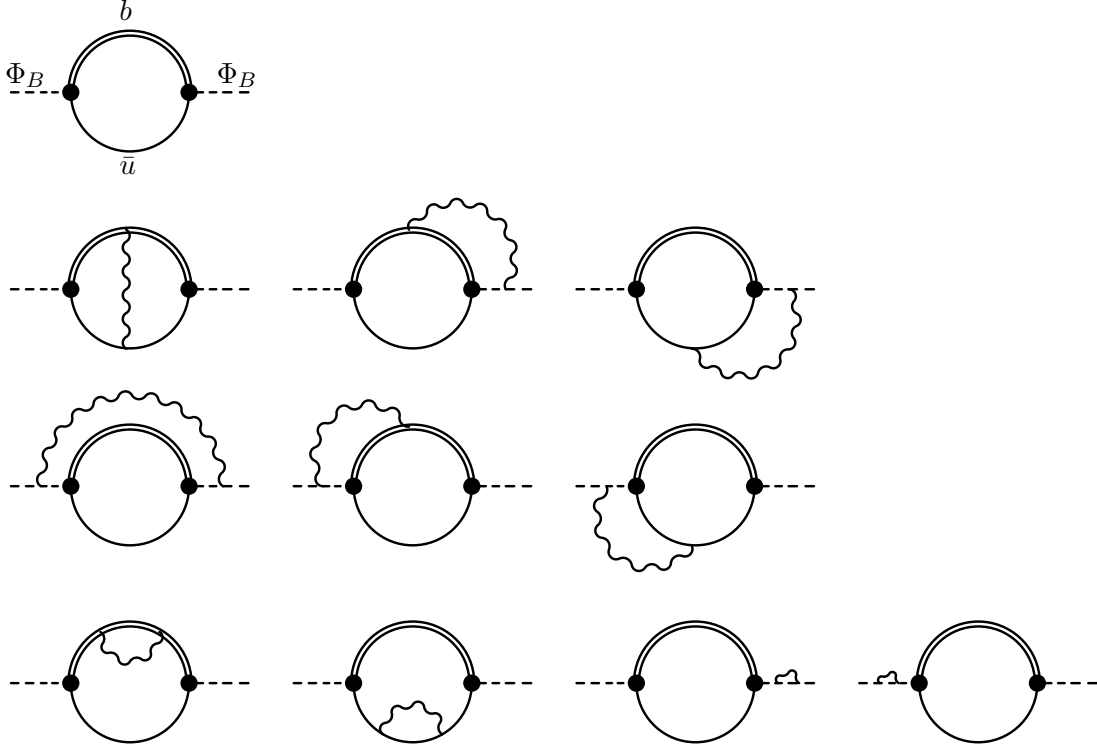


Figure 3: Diagrams contributing to $C(p_B^2, p_\Phi^2)$ (2.13), that is $|Z_B|^2$ (2.14). Again the top line is the LO contribution.

applying the Cutkosky rules [61] in (dimensional regularisation (DR) $d = 4 - 2\epsilon$) to obtain the spectral densities. The scales present are m_b, m_q, m_ℓ and m_B and their substitution allows for different flavour transitions. Below we will present the computation for the main process Π (2.4) and the denominator C (2.13) in parallel. The denominator is simpler to calculate as it is more symmetric and free of leptons. The absence of leptons mean that we do not need to track collinear logs, $\ln m_\ell$. For Π there are soft divergences and collinear logs for which a two cut-off phase space slicing technique is employed.

3.1 Leading order

The tree level result for the V-A correlator is

$$\text{Im } \Pi^{(0)}(p_B^2) = \frac{m_+^2 N_c}{8\pi} g_{\text{eff}} m_\ell \bar{u} \Gamma v \frac{\lambda_{p_B}^{\frac{1}{2}}}{p_B^2} \left(1 - \frac{m_-^2}{p_B^2}\right) \mathcal{S}(\epsilon), \quad (3.1)$$

where the zero superscripts denotes $\mathcal{O}(e^0)$ and $\mathcal{S}(\epsilon) = 1 - \epsilon \ln\left(\frac{\lambda_{p_B}}{4\mu^2 p_B^2}\right) + \epsilon(2 - \gamma_E + \ln \pi)$ gives the $\mathcal{O}(\epsilon)$ correction (γ_E is the Euler-Mascheroni constant). Both quark propagators are cut generating a Källén function of the type $\lambda_{p_B} = \lambda(p_B^2, m_b^2, m_q^2)$. Similarly the LO denominator correlator result is

$$\text{Im } C^{(0)}(p_B^2) = \frac{m_+^2 N_c}{8\pi} \lambda_{p_B}^{\frac{1}{2}} \left(1 - \frac{m_-^2}{p_B^2}\right) \mathcal{S}(\epsilon). \quad (3.2)$$

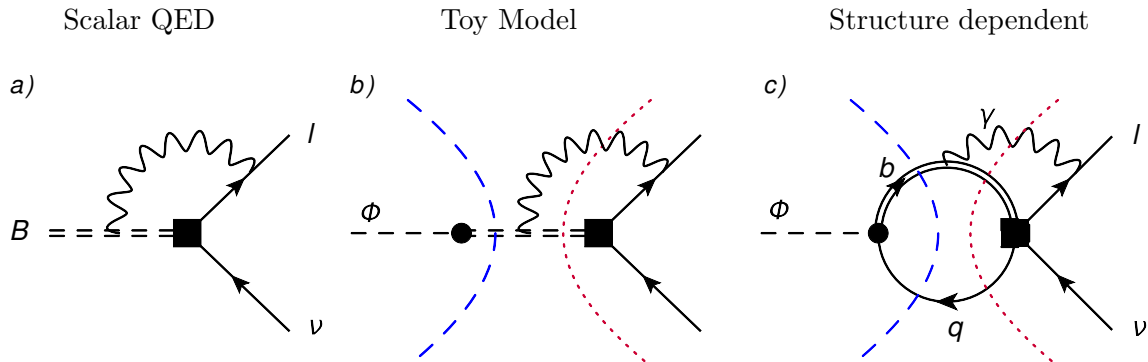


Figure 4: Virtual diagrams for the decay of a B^- -meson in increasing levels of complexity. Left (a): the decay in scalar QED where the meson is point-like. In this case there are also contact diagrams (not drawn) where the photon emerges from the weak vertex (black square). Middle (b): a toy model (cf. App. B.2) where we make use of the \mathcal{J}_B operator (black circle) but we keep the meson point-like. Right (c): the full calculation, i.e. the $b\ell_1$ contribution to $\Pi(p_B^2, p_\Phi^2)$. For (b) and (c) where there is a dispersion, the two classes of cuts in p_B^2 are shown. Those where the photon is not cut are what we refer to as blue cuts (dashed), while those where it is are the red cuts (dotted).

The two results above are similar, not by chance, since some powers of the decay constant will have to cancel.

3.2 Virtual corrections

When using Cutkosky rules to calculate the imaginary parts of the virtual diagrams the cuts fall into two classes cf. Fig. 4. Ones where the photon is not cut but the quarks are, which we refer to as the “blue cuts”, and ones where the photon is cut in addition, which we refer to as the “red cuts”.⁴ In the red cuts, as the photon is put on shell, the calculation resembles a real decay. While for the blue cuts the calculation is simplified as the photon loop factorises.

Below we will go through the procedure taking the $b\ell_1$ -diagram as an example. The Feynman integral representation of the main process assumes the form

$$\Pi_{b\ell_1}^{(2)} = \frac{-m_+ g_{\text{eff}} e^2 Q_b Q_{l_1} N_c \mu^{4\epsilon}}{(2\pi)^{2d}} \int d^d k d^d l \frac{\text{Tr}[\gamma_5(-\not{l} + m_q) \hat{\Gamma}_\mu(\not{q} - \not{l} + m_b) \gamma_\rho(p_B - \not{l} + m_b)] \bar{u} \gamma_\rho(\not{l}_1 - \not{k} + m_\ell) \Gamma_\mu v}{(l^2 - m_q^2)((p_B - l)^2 - m_b^2)((q - l)^2 - m_b^2) k^2 (l_1 - k)^2 - m_\ell^2}, \quad (3.3)$$

where we have chosen the Feynman gauge for brevity in the presentation (gauge invariance of the procedure is discussed in Sec. 3.2.2). Taking a blue cut then involves cutting the l and $p_B - l$ momentum propagators and this leads to the form

$$\text{Im} \Pi_{b\ell_1}^{(2)}|_{\text{blue}} = \frac{-2i\pi^2 m_+ g_{\text{eff}} e^2 Q_b Q_{l_1} N_c \mu^{4\epsilon}}{(2\pi)^{2d}} \int d^d l \delta^+(l^2 - m_q^2) \delta^+((p_B - l)^2 - m_b^2)$$

⁴Now, in the real emission case [42] only the blue cuts need to be taken into account when the photon is energetic. In this work we consider soft photons as well which is in any case forced upon us by the virtual diagrams which do not discriminate between hard and soft momenta.

$$\times \int d^d k \frac{\text{Tr}[\dots] \bar{u} \dots v}{((q-l)^2 - m_b^2) k^2 (l_1 - k)^2 - m_\ell^2}, \quad (3.4)$$

where the trace and spinor structures are dot-suppressed for brevity. The photon loop (in $d^d k$) factorises and can be calculated straightforwardly. The integration over $d^d l$ is less standard since one has to take into account the delta functions $\delta^+(p^2 - m^2) \equiv \theta(p^0) \delta(p^2 - m^2)$ which force the quarks on-shell. In the case of the red cuts the l , $q-l$ and k propagators are cut which leads to the following form

$$\text{Im } \Pi_{b\ell_1}^{(2)}|_{\text{red}} = \frac{-4\pi^3 m_+ g_{\text{eff}} e^2 Q_b Q_{l_1} N_c \mu^{4\epsilon}}{(2\pi)^{2d}} \int d^d k \frac{\delta^+(k^2)}{(l_1 - k)^2 - m_\ell^2} \times \int d^d l \delta^+(l^2 - m_q^2) \delta^+((q-l)^2 - m_b^2) \frac{\text{Tr}[\dots] \bar{u} \dots v}{(p_B - l)^2 - m_b^2}. \quad (3.5)$$

As noted earlier, the $\delta^+(k^2)$ -function enforces the photon to be on-shell and makes this resemble a real decay. The integrals have at most two open Lorentz indices due to the contraction with the spinor structures. The angular integration is generally quite complicated due to the many mass scales involved and the need to retain all $\mathcal{O}(\epsilon)$ -terms because the energy integrals contain soft divergences in $1/\epsilon$. Fortunately, all integrals required are known in the literature [62–64]. The calculation is simplified by choosing the p_B rest frame and exploiting systematically the symmetry between the b and q quark where possible. In the case of the bb - and qq -diagrams (in the main process and for the LSZ-factor) there is an additional technical difficulty in terms double propagators: $1/(l^2 - m_q^2)^2$. When cut this generates derivatives of delta functions, $2\pi i \delta'(l^2 - m_q^2)$, which can be dealt with by

$$\text{Im} \int \frac{1}{(l^2 - m_q^2)^2} = \lim_{N^2 \rightarrow m_q^2} \frac{d}{dN^2} \text{Im} \int \frac{1}{l^2 - N^2}, \quad (3.6)$$

commuting the Im and derivative operations. The variable N is kept distinct from m_q in order to avoid differentiation of other m_q -dependent parts. The three diagrams involving leptons are complicated by $\epsilon_{\mu\nu\rho\sigma}$ structures contracted with spinors. These can be removed via the Chisholm identity in $d = 4$ only after we have removed all poles. Using the delta functions, the diagrams are calculated analytically up until a final single numerical integral. All the diagrams have been checked numerically to per mille precision using PYSECDEC [65] to $\mathcal{O}(\epsilon^0)$.

3.2.1 Infrared sensitive (soft) terms

Here we aim to discuss infrared divergences which are of two types. The universal soft IR divergences due to the massless photon, which are well-described by scalar QED, and artificial $\ln m_q$ -terms which have to cancel in all observables. The physical collinear logs $\ln m_\ell$ originating from lepton diagrams are discussed in Sec. 4.

When taking individual cuts soft and collinear divergences proliferate which would otherwise cancel once cuts are combined. Let us first consider artificial divergences of the soft and collinear type. The former are regulated by $1/\epsilon_{\text{IR}}$ and the latter, due to the presence of an internal light quark, take on the form $\ln m_q$. Both of them must and do

cancel (between red and blue cuts) in each individual diagram. This shows the importance of taking into account all possible cuts, discussed further in App. B.1.

Let us turn to the physical IR sensitive terms. As is well-known, soft divergences are generated by at least two on-shell particles and thus in the main process the $\Phi \ell_1$ -diagram is the relevant diagram. It contains a soft divergence which only cancels against the real radiation and must be isolated as a $1/\epsilon_{\text{IR}}$ pole. The other main process diagrams only have artificial soft divergences that cancel between red and blue cuts.

The $\ln m_q$, $\ln m_\ell$ and $1/\epsilon_{\text{IR}}$ poles arise in a different manner depending on the type of cut. For the blue cuts they are generated straightforwardly from the factorised photon one-loop integration. The red cuts are technically more demanding as they cut through both loops. We adapt the phase space slicing method for the treatment of real radiation (e.g. [66]) to the virtual diagrams. Taking again the $b \ell_1$ -example in (3.5) and letting the result of the l -integral be $I_{b \ell_1}$, we obtain

$$\begin{aligned} \text{Im } \Pi_{b \ell_1}^{(2)}|_{\text{red}} &= \frac{\pi^3 m_+ g_{\text{eff}} e^2 Q_b Q_{\ell_1} N_c \mu^{4\epsilon}}{(2\pi)^{2d}} \int \frac{d^{d-1} \mathbf{k}}{|\mathbf{k}|} \frac{I_{b \ell_1}}{k \cdot l_1} \theta(q^2 - m_+^2) \\ &= \frac{\pi^3 m_+ g_{\text{eff}} e^2 Q_b Q_{\ell_1} N_c \mu^{4\epsilon}}{(2\pi)^{2d}} \int_0^\Lambda d|\mathbf{k}| \int d\Omega_{d-1} \frac{|\mathbf{k}|^{d-3}}{k \cdot l_1} I_{b \ell_1}. \end{aligned} \quad (3.7)$$

The θ function generated by the l -integral acts to cut-off the photon energy at

$$\Lambda \equiv \frac{p_B^2 - m_+^2}{2(p_B^2)^{1/2}}. \quad (3.8)$$

The $k \cdot l_1$ denominator gives the $\ln m_\ell$ -terms when \mathbf{k} and \mathbf{l}_1 are parallel, while there is a soft divergence since $I_{b \ell_1} \sim 1/|\mathbf{k}|$ for $|\mathbf{k}| \rightarrow 0$. In the slicing procedure we decompose the photon energy integral into a soft part, treated in $d = 4 - 2\epsilon$, and a hard part in $d = 4$

$$\int_0^\Lambda d|\mathbf{k}| \int d\Omega_{d-1} \rightarrow \int_0^{\Delta E_s} d|\mathbf{k}| \int d\Omega_{d-1} + \int_{\Delta E_s}^\Lambda d|\mathbf{k}| \int d\Omega_3. \quad (3.9)$$

The boundary between the two regions is ΔE_s , and chosen to be sufficiently small to drop subleading powers of $|\mathbf{k}|$ in the soft integrand. The hard part is to be further decomposed into collinear and non-collinear sections (cf. Sec. 4.2).

In order to illustrate the soft pole we have to turn to the $\Phi \ell_1$ -diagram

$$\text{Im } \Pi_{\Phi \ell_1}^{(2)} = \frac{\alpha}{4\pi} Q_\Phi Q_{\ell_1} \frac{m_B^2 + m_\ell^2}{m_B^2 - m_\ell^2} \ln \left(\frac{m_B^2}{m_\ell^2} \right) \frac{\text{Im } \Pi^{(0)}(p_B^2)}{\epsilon_{\text{IR}}} + \mathcal{O}(\epsilon^0), \quad (3.10)$$

which matches the universal soft results [7, 8] and cancels against the real radiation after Borel transformation. Note that the expression above contains both a soft pole and a collinear log. There are additional soft-collinear terms $\ln^2 m_\ell$ of the same origin which cancel similarly. Note that the separation of the soft region is frame dependent due to the ΔE_s (defined in the p_B rest frame) but since the final results are finite in the $\Delta E_s \rightarrow 0$ limit this is of no concern.

In the denominator the only soft divergent one-particle irreducible (1PI) diagram is the $\Phi\Phi$ -diagrams as it is the only diagram without a blue cut

$$\text{Im } C_{\Phi\Phi}^{(2)} = \frac{\alpha}{2\pi} Q_\Phi^2 \frac{\text{Im } C^{(0)}(p_B^2)}{\epsilon_{\text{IR}}} + \mathcal{O}(\epsilon^0). \quad (3.11)$$

IR-finiteness is achieved by taking into account the Φ self energy in the on-shell scheme (cf. Sec. 3.2.3).

3.2.2 Gauge invariance

In the explicit computation the Feynman gauge, $\xi = 1$, was assumed. Here we turn to the question of gauge invariance by tracking the $(\xi - 1)k_\mu k_\nu / (k^2)^2$ -terms. Whereas these have $1/k^4$ -parts, they are simplified as Ward identities contract propagators to a point. The blue cuts vanish separately for each diagram in DR while the red cuts cancel by charge conservation $Q_\Phi = Q_{\ell_1} = Q_b - Q_q$. Explicitly, gauge invariance for the (1PI) diagrams reads

$$\begin{aligned} \text{Im } \Pi^{(2)}|_{1-\xi} &= \frac{4\pi^4 m_+^2 g_{\text{eff}} e^2 N_c \mu^{4\epsilon}}{(2\pi)^{2d}} \left(Q_{\ell_1} (Q_\Phi - Q_b + Q_q) - Q_\Phi (Q_b - Q_q) + (Q_b - Q_q)^2 \right) \\ &\times \lim_{N^2 \rightarrow 0} \frac{d}{dN^2} \int d^d k \delta^+(k^2 - N^2) \theta(q^2 - m_+^2) \bar{u} q \Gamma v \frac{\lambda_q^{\frac{1}{2}}}{q^2} \left(1 - \frac{m_-^2}{q^2} \right) = 0, \end{aligned} \quad (3.12)$$

since the bracket of charges vanishes, and equally so for the denominator

$$\begin{aligned} \text{Im } C^{(2)}|_{1-\xi} &= \frac{2\pi e^2 \mu^{2\epsilon}}{(2\pi)^d} \left(Q_\Phi^2 - 2Q_\Phi (Q_b - Q_q) + (Q_b - Q_q)^2 \right) \\ &\times \lim_{N^2 \rightarrow 0} \frac{d}{dN^2} \int d^d k \delta^+(k^2 - N^2) \theta(q^2 - m_+^2) \text{Im } C^{(0)}(q^2) = 0, \end{aligned} \quad (3.13)$$

where $\lambda_q = \lambda(q^2, m_b^2, m_q^2)$. Note that the first equation has the same structure as the LO expression with $p_B^2 \rightarrow q^2$ which is related to the Ward identity statement above.

3.2.3 Renormalisation

In addition to IR divergences there are ultraviolet (UV) divergences with some of them being peculiar to QED. For example, the J_B -operator which is renormalisation group invariant in QCD, renormalises in QED due to $Q_b \neq Q_q$. In $\overline{\text{MS}}$ we obtain that \mathcal{J}_B (2.1), setting $m_q = 0$, renormalises as⁵

$$\begin{aligned} Z_{\Phi_B J_B} &= 1 + \frac{\alpha}{4\pi \hat{\epsilon}_{\text{UV}}} \left(- (3 + \xi) Q_b Q_q - \xi Q_\Phi (Q_b - Q_q) + \frac{1}{2} \xi (Q_b^2 + Q_q^2) - \frac{1}{2} (3 - \xi) Q_\Phi^2 + 3Q_b^2 \right) \\ &= 1 + \frac{3\alpha}{8\pi \hat{\epsilon}_{\text{UV}}} (Q_b^2 - Q_q^2), \end{aligned} \quad (3.14)$$

where we made use of charge conservation in the second line. For $Q_q = Q_b$ one recovers the non-renormalisation of J_B in QCD.

⁵For convenience, we define $\frac{1}{\epsilon} = \frac{1}{\epsilon} - \gamma_E + \ln 4\pi$.

Turning to our computation matters are slightly complicated since we keep both m_q and m_b non-zero and this leads to non-multiplicative renormalisation. All 1PI renormalisations are performed in $\overline{\text{MS}}$, except for the b -quark mass for which we considered several options but found the kinetic scheme to give the most stable results (cf. Sec. 5). The self energy (SE) corrections of the external particles are handled, as usual, in the on-shell scheme (e.g. [67])

$$\begin{aligned}\text{Im } \Pi_{\text{SE}}^{(2)} &= \frac{\alpha}{2\pi} \left(Q_{\Phi}^2 \delta Z_S + Q_{\ell_1}^2 \delta Z_2 \right) \text{Im } \Pi^{(0)}(p_B^2), \\ \text{Im } C_{\text{SE}}^{(2)} &= \frac{\alpha}{\pi} Q_{\Phi}^2 \delta Z_S \text{Im } C^{(0)}(p_B^2),\end{aligned}\tag{3.15}$$

with scalar and fermion Z factors

$$\begin{aligned}4 \delta Z_S &= (3 - \xi) \left(\frac{1}{\hat{\epsilon}_{\text{UV}}} - \frac{1}{\hat{\epsilon}_{\text{IR}}} \right) + 1 - \xi, \\ 4 \delta Z_2 &= -\xi \frac{1}{\hat{\epsilon}_{\text{UV}}} - (3 - \xi) \frac{1}{\hat{\epsilon}_{\text{IR}}} + 3 \ln \left(\frac{m_{\ell}^2}{\mu^2} \right) - (3 + \xi),\end{aligned}\tag{3.16}$$

using the expression in Eq. 2.18 in [9]. It is implicitly understood that we adapt the same scheme choice for the main process and the LSZ-factor to enable necessary cancellations to occur.

Finally there is the issue of the running of the weak 4-Fermi operator in (2.5). Some of the QED-corrections are absorbed into the definition of G_F (taken from muon decay) using the W-regularisation [68]. As we regulate in DR this procedure must be adapted as done in [69–71]. It amounts to the replacement $G_F \rightarrow G_F C(\mu)$ with

$$C(\mu) = 1 + \frac{\alpha}{2\pi} \left(\ln \left(\frac{M_Z^2}{\mu^2} \right) - \frac{11}{6} \right).\tag{3.17}$$

3.2.4 Final virtual rate

After renormalisation, the denominator C is IR and UV finite and $|\mathcal{Z}_B|^2$ can be extracted through (2.14). For the main process we must first square the amplitude, spin sum and integrate over (the trivial) phase space. Defining $\text{Im } \Pi = \text{Im } \overline{\Pi} \bar{u} \Gamma v$ and $\mathcal{B}_{M^2} \Pi = \frac{1}{\pi} \int ds \text{Im } \Pi(s) e^{(m_B^2 - s)/M^2}$, the virtual rate reads

$$\begin{aligned}\left[|\mathcal{Z}_B|^2 \Gamma_{B \rightarrow \ell \bar{\nu}} \right] &= \frac{(m_B^2 - m_{\ell}^2)^2}{4\pi \mu^2 \epsilon m_B^3} \left((\mathcal{B}_{M^2} \overline{\Pi}^{(0)}) (\mathcal{B}_{M^2} \overline{\Pi}^{(0)})^* \right. \\ &\quad \left. + 2\mathcal{K}(\epsilon) \text{Re} (\mathcal{B}_{M^2} \overline{\Pi}^{(2)}) (\mathcal{B}_{M^2} \overline{\Pi}^{(0)})^* + \mathcal{O}(\alpha^2) \right),\end{aligned}\tag{3.18}$$

where the first and second term correspond to the LO- and the NLO-result. The quantity $\mathcal{K}(\epsilon) = 1 - 2\epsilon \ln \frac{m_B^2 - m_{\ell}^2}{2\mu m_B} + \epsilon(2 - \gamma_E + \ln \pi)$ parametrises phase space corrections which cancel against the real radiation and so in practise can be ignored.

3.3 Real radiation

3.3.1 The amplitude

The calculation of the amplitude $\mathcal{A}(B^- \rightarrow \ell^- \bar{\nu} \gamma)$ involves three pieces which we may write schematically (cf. (2.10) for the relation to the amplitude) as follows

$$\Pi_\rho^\gamma(p_B^2, q^2) = \Pi_\rho^\gamma|_{\text{lep}} + \Pi_\rho^\gamma|_\Phi + \Pi_\rho^\gamma|_B, \quad (3.19)$$

with ρ to be contracted with the photon polarisation tensor, ϵ_ρ^* . The first and second term are the leptonic and the Φ particle contributions. Since both sets of particles are treated as point-like they are straightforward. The third is non-trivial as it is truly structure-dependent and for which we adapt (cf. below (2.11)) the NLO LCSR computation [42]. In that reference the point-like contributions (contact terms) were separated from the truly structure-dependent part and we may thus write, using the shorthand (g_{eff} defined in (2.6) and $q = p_B - k$)

$$\tilde{g} \equiv m_+ g_{\text{eff}} e s_e, \quad (3.20)$$

in the Lorentz gauge^{6,7}

$$\Pi_\rho^{(\gamma)}|_{\text{lep}} = \tilde{g} Q_{\ell_1} \Pi_{f_B}(p_B^2) \left(\bar{u} \gamma_\rho \Gamma v + \frac{m_\ell}{2l_1 \cdot k} \left(\bar{u} \gamma_\rho \not{k} \Gamma v + 2(l_1)_\rho \bar{u} \Gamma v \right) \right), \quad (3.21)$$

$$\Pi_\rho^{(\gamma)}|_\Phi = -\tilde{g} Q_\Phi \frac{(p_\Phi)_\rho}{p_\Phi \cdot k} \Pi_{f_B}(q^2) m_\ell \bar{u} \Gamma v,$$

$$\Pi_\rho^{(\gamma)}|_B = \tilde{g} Q_\Phi \bar{u} \Gamma^\mu v \left(\frac{\Pi_{f_B}(q^2) - \Pi_{f_B}(p_B^2)}{k \cdot p_B} (p_B)_\rho (p_B)_\mu - \Pi_{f_B}(q^2) g_{\rho\mu} \right) + \Pi_\rho^{(\gamma)}|_B^{\text{struc}},$$

where we have separated the structure-dependent part which depends on the quark charges in a non-trivial manner. The correlation function $\Pi_{f_B}(p^2)$ is related to the tree level correlator via $\Pi^{(0)}(p_B^2) = g_{\text{eff}} m_+ m_\ell \bar{u} \Gamma v \Pi_{f_B}(p_B^2)$ defined in (3.1). It is noted that the function arguments differ in the Φ - and lepton-case because the photon is radiated before (q^2) versus after (p_B^2) the B -meson is resolved respectively. Finally, the structure-dependent part is contained in two form factors $V_{\perp, \parallel}$ defined from [42]

$$\langle \gamma | \bar{q} \hat{\Gamma}_\mu b | B \rangle = -\frac{s_e e}{m_B} \left(P_\mu^\perp V_\perp(q^2) - P_\mu^\parallel (V_\parallel(q^2) + Q_{B^-} \frac{m_B f_B}{k \cdot p_B}) - P_\mu^{\text{Low}} Q_{B^-} \frac{m_B f_B}{k \cdot p_B} \right), \quad (3.22)$$

where $P^\mu \equiv P^{\mu\rho} \epsilon_\rho^*(k)$ with

$$P_{\mu\rho}^\perp \equiv \varepsilon_{\mu\rho\beta\gamma} (p_B)^\beta k^\gamma, \quad P_{\mu\rho}^\parallel \equiv i(k \cdot p_B g_{\mu\rho} - k_\mu (p_B)_\rho), \quad P_{\mu\rho}^{\text{Low}} \equiv i(p_B)_\mu (p_B)_\rho. \quad (3.23)$$

Assembling all parts we obtain the amplitude (using (2.10))

$$m_+(\mathcal{A}^\gamma)^\rho = -i\tilde{g} Q_{\ell_1} F_B \left(\bar{u} \gamma^\rho \Gamma v + \frac{m_\ell}{2l_1 \cdot k} \left(\bar{u} \gamma^\rho \not{k} \Gamma v + 2l_1^\rho \bar{u} \Gamma v \right) \right) + \frac{\tilde{g} Q_\Phi F_B}{k \cdot p_B} P_{\text{Low}}^{\mu\rho} \bar{u} \Gamma_\mu v$$

⁶The flag $s_e = \pm 1$ corresponds to the convention of the covariant derivative cf. App. A. It is important to keep track of it when combining the form factor contribution with the Φ -emission diagram.

⁷The structure-dependent part, is given by $\Pi_\rho^{(\gamma)}|_B^{\text{struc}} = (\tilde{g}/im_+m_B) \bar{u} \Gamma^\mu v (\Pi_\perp^V P_{\mu\rho}^\perp - \Pi_\parallel^V P_{\mu\rho}^\parallel)$, with $\Pi_{\perp, \parallel}^V$ given in [42]. Note that here (the charged case), the form factors $V_{\perp, \parallel}$ are negative.

$$- \frac{\tilde{g}}{m_B} \left(V_{\perp}(q^2) P_{\perp}^{\mu\rho} - \left(V_{\parallel}(q^2) + \frac{Q_{\Phi} m_B F_B}{k \cdot p_B} \right) P_{\parallel}^{\mu\rho} \right) \bar{u} \Gamma_{\mu} v, \quad (3.24)$$

where as before non-physical Lorentz structures proportional to r are discarded, and r is effectively set to zero everywhere except in F_B , the sum rule equivalent of f_B (1.1),

$$F_B = F_B(M^2) \equiv \frac{m_{\pm}}{\mathcal{Z}_B} \mathcal{B}_{M^2} \Pi_{f_B}(p_B^2), \quad (3.25)$$

in the sense that $p_B^2 \neq m_B^2$. These terms proportional to F_B must be included in this way in order to guarantee the cancellation of the soft IR divergences. Importantly a term in the $P_{\parallel}^{\mu\rho}$ -structure of the type $(\Pi_{f_B}(p_B^2) - \Pi_{f_B}(q^2))/(p_B^2 - q^2)$, required by the equation of motion, has been dropped since this term is automatically absorbed into the very definition of V_{\parallel} (3.22), in [42]. The correspondence between (3.22) and (3.24) is established by $Q_{\Phi} = Q_{B^-}$ (with the addition of the lepton parts) and for $m_{\ell} \rightarrow 0$ one recovers the well known result that the amplitude is expressed entirely in terms of the form factors. All other terms in (3.24) correspond to the point-like approximation. Note that the $V_{\perp} P_{\perp}$ and $V_{\parallel} P_{\parallel}$ -terms are of $\mathcal{O}(E_{\gamma})$ whereas all the remaining terms are of order $\mathcal{O}(1/E_{\gamma})$ or $\mathcal{O}((E_{\gamma})^0)$ which are universal due to Low's theorem. Gauge invariance, $k \cdot \mathcal{A}^{\gamma} = 0$, of (3.24) follows from applying charge conservation $Q_{\Phi} = Q_{\ell_1}$ and $k^{\rho} P_{\mu\rho}^{\parallel,\perp} = 0$.

Finally, we consider it worthwhile to comment on the role of what we called blue (p_B^2) and red (q^2) cuts. These cuts start at

$$p_B^2|_{\text{blue}} > m_{\pm}^2, \quad p_B^2|_{\text{red}} > (E_{\gamma} + \sqrt{E_{\gamma}^2 + m_{\pm}^2})^2, \quad (3.26)$$

respectively. In the LCSR computation [42] which is valid at large recoil ($E_{\gamma} > 1.25 \text{ GeV}$ or $q^2 < 14 \text{ GeV}^2$), the red cuts never contribute and are simply not necessary [14].⁸

3.3.2 Final radiative rate

To infer the rate $\Gamma^{B \rightarrow \ell \bar{\nu} \gamma}$, the correlator must be Borel transformed, leading to $i\mathcal{A}^{\gamma} \mathcal{Z}_B$, which is then squared and integrated over the three body phase space. Note that only Π_{f_B} and not the Lorentz structures are Borel transformed in line with the dispersion relations. In the Lorentz structures $p_B^2 \rightarrow m_B^2$ is assumed. The phase space integration for the real rate reads

$$\begin{aligned} \left[|\mathcal{Z}_B|^2 \Gamma_{B \rightarrow \ell \bar{\nu} \gamma} \right] &= \frac{(2\pi)^d}{2m_B} \int \left[\langle |\mathcal{A}^{\gamma}|^2 \rangle |\mathcal{Z}_B|^2 \right] \delta^{(d)}(p_B - l_1 - l_2 - k) \\ &\times \frac{d^{d-1} \mathbf{l}_1}{(2\pi)^{d-1} 2E_{l_1}} \frac{d^{d-1} \mathbf{l}_2}{(2\pi)^{d-1} 2E_{l_2}} \frac{d^{d-1} \mathbf{k}}{(2\pi)^{d-1} 2E_{\gamma}}, \end{aligned} \quad (3.27)$$

where $\langle \dots \rangle$ indicates that spin and polarisation sums have been performed. Again, it is convenient to work in the p_B rest frame. The soft part of the integral is treated with a

⁸We can make this discussion more concrete by focusing on the Low-type terms (second and third line) in (3.21). In the LCSR computation the Low term is corresponds to $\Pi_{f_B}(p_B^2)(p_B)^{\rho}(p_B)^{\mu}$ on the third line. Here however the Low term comes from the second line and the entire third line is subleading in the photon energy (since $p_B^2 \approx q^2$).

conventional real slicing technique to obtain

$$\begin{aligned} \left[\Gamma_{B \rightarrow \ell \bar{\nu} \gamma} \right]_{\text{soft}} = & - \frac{\tilde{g}^2 m_\ell^2 (m_B^2 - m_\ell^2)^2}{16\pi^3 m_B^3 m_+^2 \mu^{2\epsilon}} F_B^2 \mathcal{K}(\epsilon) \left[\frac{1}{2} Q_{\ell_1}^2 \frac{m_B^2 + m_\ell^2}{m_B^2 - m_\ell^2} \ln \frac{m_\ell^2}{m_B^2} \right. \\ & \left. + \left(\frac{-1}{2\hat{\epsilon}_{\text{IR}}} + \ln \frac{m_B \omega_s^\gamma}{\mu} \right) \left(Q_\Phi^2 + Q_{\ell_1}^2 + Q_\Phi Q_{\ell_1} \frac{m_B^2 + m_\ell^2}{m_B^2 - m_\ell^2} \ln \frac{m_\ell^2}{m_B^2} \right) + \dots \right], \end{aligned} \quad (3.28)$$

with F_B as in (3.25). The dots stand for finite contributions or soft collinear terms which cancel with the virtual. Notice that there is a finite $Q_\ell^2 \ln m_\ell$ -term generated from this soft region, shown explicitly in (3.28). Again the $1/\epsilon_{\text{IR}}$ pole is universal and cancels with the virtual provided that the same sum rule specific parameters s_0, M^2 are chosen. The soft cut-off $\omega_s^\gamma \equiv 2(\Delta E_s^\gamma)/m_B$ dependence cancels against the hard region. The hard integration (for which one can assume $d = 4$) is easily performed using the Dalitz variables

$$x = 1 - \frac{(p_B - k)^2}{m_B^2}, \quad y = 1 - \frac{(p_B - l_1)^2}{m_B^2}, \quad (3.29)$$

where x and y serve as dimensionless photon energy and angular integration variables. Explicitly the hard integration assumes the form

$$\left[|\mathcal{Z}_B|^2 \Gamma_{B \rightarrow \ell \bar{\nu} \gamma} \right]_{\text{hard}} = \frac{m_B}{256\pi^3} \int_{\omega_s^\gamma}^{r_E} dx \int_{1-x+\frac{xm_\ell^2}{(1-x)m_B^2}}^1 dy \left[\langle |\mathcal{A}^\gamma|^2 \rangle |\mathcal{Z}_B|^2 \right]. \quad (3.30)$$

The photon energy cut-off is parameterised by $r_E \equiv 2E_\gamma^{\text{cut}}/m_B \in [0, 1 - m_\ell^2/m_B^2]$. (Hard) collinear divergences arising from the angular integration over the photon-lepton angle $c_\gamma = \cos \theta$ (defined in the B rest frame) are discussed in the next section.

4 Collinear logs

We now turn to one of the central conceptual points of the paper and that is the structure-dependent collinear logs in m_ℓ . As discussed in the introduction, their appearance for V-A interactions in leptonic decays is rather the exception than the rule as it is owed to the chiral suppression of the tree-level amplitude. For example, the computation of the $B_s \rightarrow \mu^+ \mu^-$ virtual structure-dependent corrections in SCET show such logs (cf. Eq. 5 in [31]) but what seems not to have been appreciated is that they are specific to that decay with V-A interactions. These logs must be absent in Yukawa-type S-P interactions as shown by our explicit computation below.

4.1 Universal IR logs from the splitting function

We consider it worthwhile to illustrate the universality of the collinear logs in the case where the KLN-theorem applies. The point is that the KLN-theorem is based on unitarity which in turn implies that collinear logs $\ln m_\ell$ must cancel between real and virtual parts. In that case they are reproducible from the splitting function and the LO decay rate e.g. [13]. This has been exploited to infer the QED-effects on the charmonium resonances in the low $q^2 = (l_+ + l_-)^2$ region in $B \rightarrow K \ell^+ \ell^-$ [10]. The point is that in the SM $B \rightarrow K \ell^+ \ell^-$,

unlike the leptonic decay, is not chirally suppressed. Hence, the non-chirally suppressed S-P case can be treated in the same way using the splitting function⁹

$$P_{f \rightarrow f\gamma}(z) = \frac{1+z^2}{(1-z)_+} + \frac{3}{2}\delta(1-z), \quad (4.1)$$

where (cf. (3.29))

$$z = 1 - x = \frac{(p_B - k)^2}{m_B^2}, \quad (4.2)$$

takes the value $z = 1$ when the photon is soft. The result yields [13]

$$\begin{aligned} \Gamma_{\text{S-P}}^{\text{NLO}}|_{\ln m_\ell} &= -\frac{\alpha}{\pi} Q_{\ell^-}^2 \ln m_\ell \int_{1-r_E}^1 dz P_{f \rightarrow f\gamma}(z) \Gamma_{\text{S-P}}^{\text{LO}} \\ &= -\frac{\alpha}{\pi} Q_{\ell^-}^2 \ln m_\ell \left(\frac{3}{2} - r_E \left(2 - \frac{1}{2} r_E \right) \right) \Gamma_{\text{S-P}}^{\text{LO}}, \end{aligned} \quad (4.3)$$

for the collinear logs with photon energies up to the energy cut-off r_E . When fully inclusive in the photon energy, $r_E \rightarrow 1$, the logs cancel completely. This is a rather simple example as for more involved kinematics such as $B \rightarrow K \ell^+ \ell^-$ the LO rate depends on the collinear momentum fraction z [10]. Our point is that we expect (4.3) to hold for the S-P case but not the V-A case. In what follows we will verify this explicitly using the slicing technique.

4.2 The virtual contribution

In general, hard-collinear (hc) logs can be generated from both the red and blue cuts in the virtual case. The blue cuts as emphasised previously are simple since they reduce to one-loop functions. As the red cuts involve an on-shell photon integration, due to the cut photon propagator, the extraction of the collinear part is complicated. As a new feature, we adapt the slicing method, from the real radiation, to the virtual collinear case.¹⁰ We parameterise the virtual collinear region by $\{z_v, k \cdot l_1\}$ where

$$k = (1 - z_v) l_1, \quad (4.4)$$

such that $(1 - z_v)$ is proportional to virtual photon energy. The collinear phase space in the hard regime ($d = 4$) becomes

$$\int_{\text{hc}} \frac{d^3 \mathbf{k}}{|\mathbf{k}|} = 2\pi \int_{\delta_H}^{1-\omega_s} dz_v \int_{\frac{1}{2}(1-z_v)m_\ell^2}^{\omega_c p_B^2} d(l_1 \cdot k), \quad (4.5)$$

where

$$\omega_s \equiv \frac{2\Delta E_s}{(p_B^2)^{1/2}}, \quad \delta_H \equiv \frac{m_+^2}{p_B^2}, \quad (4.6)$$

⁹The $1/(1-z)_+$ is the plus distribution, defined under the integral as $\int_0^1 dz f(z)/(1-z)_+ \equiv \int_0^1 dz (f(z) - f(1))/(1-z)$, which regulates the soft region $z \rightarrow 1$.

¹⁰We are not aware as to whether this has been done previously in the literature. We however have not conducted an extensive search.

are the dimensionless soft (removing the universal soft-region) and hard (the dimensionless equivalent of Λ (3.8)) cut-offs. The collinear logs arise from $1/l_1 \cdot k$ -terms in the integrand and are regulated by m_ℓ^2 in the lower integration limit. The upper limit $\omega_c \ll \omega_s$ is a dimensionless collinear cut-off which will cancel against the hard non-collinear part and is of no special significance. We consider first the S-P and then the V-A case. Comparison to (4.3) requires the inclusion of the real part and postponed to the next section.

The S-P case: The blue cuts are found to match scalar QED,

$$\begin{aligned} \text{Im } \Pi_{\text{S-P}}(p_B^2)|_{\text{hc}}^{\text{blue}} &= -\frac{\alpha}{\pi} Q_{\ell_1} (Q_b - Q_q) \text{Im } \Pi_{\text{S-P}}^{(0)}(p_B^2) \ln m_\ell \\ &= -\frac{\alpha}{\pi} \text{Im } \Pi_{\text{S-P}}^{(0)}(p_B^2) \ln m_\ell, \end{aligned} \quad (4.7)$$

and in fact there cannot be complete cancellation as there are only two diagrams proportional to Q_b and Q_q respectively. This aspect changes for the red cuts which additionally have the $\Phi \ell_1$ -diagram (proportional to Q_Φ). Then cancellation can and does occur

$$\text{Im } \Pi_{\text{S-P}}(p_B^2)|_{\text{hc}}^{\text{red}} = \frac{\alpha}{\pi} Q_{\ell_1} Q_{\mathcal{J}_B} \ln m_\ell \int_{\delta_H}^{1-\omega_s} dz_v \frac{z_v}{1-z_v} \text{Im } \Pi_{\text{S-P}}^{(0)}(z_v p_B^2) = 0, \quad (4.8)$$

by $Q_{\mathcal{J}_B} = 0$ (2.2).¹¹ These aspects work very differently in the V-A case.

The V-A case: The blue cuts read

$$\begin{aligned} \text{Im } \Pi_{\text{V-A}}(p_B^2)|_{\text{hc}}^{\text{blue}} &= \frac{m_+ g_{\text{eff}} \alpha Q_{\ell_1} N_c}{16\pi^2} \frac{m_\ell \bar{u} \Gamma v}{p_B^4} \left(\right. \\ &\quad \left. Q_b \left[2m_+ m_-^2 \lambda_{p_B}^{\frac{1}{2}} + (m_+ + m_-)(p_B^2 - m_-(m_+ + m_-)) p_B^2 L^+ \right] \right. \\ &\quad \left. - Q_q \left[2m_-(m_+ m_- - p_B^2) \lambda_{p_B}^{\frac{1}{2}} + m_-(m_+ - m_-)^2 p_B^2 L^- \right] \right) \ln m_\ell, \end{aligned} \quad (4.9)$$

where

$$L^\pm = \ln \left(\frac{p_B^2 \pm m_+ m_- + \lambda_{p_B}^{\frac{1}{2}}}{p_B^2 \pm m_+ m_- - \lambda_{p_B}^{\frac{1}{2}}} \right). \quad (4.10)$$

For later convenience, define L_q^\pm as L^\pm with $p_B^2 \rightarrow q^2$. This time we do not find a result proportional to the LO results. In the $m_q \rightarrow 0$ limit the result simplifies to

$$\begin{aligned} \text{Im } \Pi_{\text{V-A}}(p_B^2)|_{\text{hc}}^{\text{blue}} &= \frac{m_b^2 g_{\text{eff}} \alpha Q_{\ell_1} N_c}{8\pi^2} \frac{m_\ell \bar{u} \Gamma v}{p_B^4} \ln m_\ell \times \\ &\quad \left(Q_b \left[m_b^2 (p_B^2 - m_b^2) + p_B^2 (p_B^2 - 2m_b^2) \ln \frac{p_B^2}{m_b^2} \right] + Q_q (p_B^2 - m_b^2)^2 \right). \end{aligned} \quad (4.11)$$

¹¹Further, since the blue cuts in the hard collinear region reproduce all universal $\ln m_\ell$ -terms and the red cuts cancel, the same must hold for any hard-collinear logs generated in the soft region. That is, there can be no other hard-collinear logs, and that is what we find explicitly with the same $Q_{\mathcal{J}_B} = 0$ cancellation occurring in the soft region. Since the soft region does not discriminate between S-P and V-A interactions this holds for V-A as well.

For the red cuts, the same cancellation by charge occurs for the soft region ($z_v \rightarrow 1$) as in the S-P case, however there *are* extra terms arising from non-soft virtual photons.

$$\begin{aligned} \text{Im } \Pi_{\text{V-A}}(p_B^2)|_{\text{hc}}^{\text{red}} &= \frac{\alpha}{\pi} Q_{\ell_1} Q_{\mathcal{J}_B} \ln m_\ell \int_{\delta_H}^{1-\omega_s} \frac{z_v}{1-z_v} \text{Im } \Pi_{\text{V-A}}^{(0)}(z_v p_B^2) dz_v \\ &\quad - \frac{m_+ g_{\text{eff}} \alpha Q_{\ell_1} N_c}{8\pi^2} m_\ell \ln m_\ell \bar{u} \Gamma v \int_{\delta_H}^{1-\omega_s} f_{\text{hc}}(z_v, p_B^2) dz_v \\ &= - \frac{m_+ g_{\text{eff}} \alpha Q_{\ell_1} N_c}{8\pi^2} m_\ell \ln m_\ell \bar{u} \Gamma v \int_{\delta_H}^1 f_{\text{hc}}(z_v, p_B^2) dz_v, \end{aligned} \quad (4.12)$$

where

$$\begin{aligned} f_{\text{hc}}(z_v, p_B^2) &= \lambda_q^{\frac{1}{2}} \left[(Q_b - Q_q) \frac{m_+ m_-^2 - p_B^2 (m_+ + m_-)}{p_B^4 z_v} + \frac{2Q_b m_- + (Q_b - Q_q) m_+}{p_B^2} \right] \\ &\quad - \frac{m_-}{2p_B^2} \left[Q_b (m_+ + m_-)^2 L_q^+ + Q_q (m_+ - m_-)^2 L_q^- \right] + Q_b (m_+ + m_-) (1 - z_v) L_q^+, \end{aligned} \quad (4.13)$$

and note that in the collinear region $q^2 = z_v p_B^2$. The function f_{hc} is not soft divergent and this justifies neglecting ω_s in (4.12). The extra parts beyond the S-P are structure-dependent contributions. The integral may easily be performed in the $m_q \rightarrow 0$ limit giving

$$\begin{aligned} \text{Im } \Pi_{\text{V-A}}(p_B^2)|_{\text{hc}}^{\text{red}} &= \frac{m_b^2 g_{\text{eff}} \alpha Q_{\ell_1} N_c}{16\pi^2} \frac{m_\ell \bar{u} \Gamma v}{p_B^4} \ln m_\ell \times \\ &\quad \left[(p_B^2 - m_b^2) (4Q_b (p_B^2 - m_b^2) + Q_q (m_b^2 - 3p_B^2)) + 2(Q_b (m_b^4 - p_B^4) + Q_q m_b^2 (2p_B^2 - m_b^2)) \ln \frac{p_B^2}{m_b^2} \right]. \end{aligned}$$

We can then combine this with the result of the blue cuts, Eq. (4.9), which yields the total 1PI hard-collinear logs ($m_q = 0$)

$$\begin{aligned} \text{Im } \Pi_{\text{V-A}}|_{\text{hc}} &= \frac{m_b^2 g_{\text{eff}} \alpha Q_{\ell_1} N_c}{16\pi^2} \frac{m_\ell \bar{u} \Gamma v}{p_B^4} \ln m_\ell \times \\ &\quad \left[(p_B^2 - m_b^2) (p_B^2 (4Q_b - Q_q) - m_b^2 (2Q_b + Q_q)) + 2m_b^2 (Q_b - Q_q) (m_b^2 - 2p_B^2) \ln \frac{p_B^2}{m_b^2} \right] \\ &= \frac{m_b^2 g_{\text{eff}} N_c \alpha}{8\pi^2} \frac{m_\ell \bar{u} \Gamma v}{p_B^4} \left(p_B^2 (p_B^2 - m_b^2) + m_b^2 (m_b^2 - 2p_B^2) \ln \frac{p_B^2}{m_b^2} \right) \ln m_\ell, \end{aligned} \quad (4.14)$$

where in the last line we have applied $Q_b = -1/3, Q_q = 2/3$. The total virtual $\ln m_\ell$ also includes the contribution from the lepton wave function renormalisation (Z_2), which from (3.15) is $(3\alpha/4\pi) Q_{\ell_1}^2 \text{Im } \Pi^{(0)} \ln m_\ell$. In order to conclude we must analyse the real radiation.

4.3 The real radiation

In the real case, collinear logs arise from the integration of inverse powers of $k \cdot l_1 = \frac{1}{2} m_B^2 (x + y - 1)$ over the angular variable y in (3.30). In the S-P case, where there is no structure-dependent form factors $V_{\parallel, \perp}(z)$, the angular integration over y can be performed and with z defined in (4.2) we obtain

$$\left[|\mathcal{Z}_B|^2 \Gamma_{B \rightarrow \ell \bar{\nu} \gamma} \right]_{\text{hc}}^{\text{S-P}} = - \frac{m_B \tilde{g}^2 Q_{\ell_1}^2}{16\pi^3} (\mathcal{B}_{M^2} \Pi_{f_B}^{\text{S-P}}(p_B^2))^2 \int_{1-r_E}^{1-\omega_s^2} \tilde{P}_{f \rightarrow f \gamma}(z) dz \ln m_\ell$$

$$r_E \xrightarrow{1} \frac{m_B \tilde{g}^2 Q_{\ell_1}^2}{16\pi^3} (\mathcal{B}_{M^2} \Pi_{f_B}^{\text{S-P}}(p_B^2))^2 \left[\frac{3}{2} + 2 \ln \omega_s^\gamma \right] \ln m_\ell + \mathcal{O}(\omega_s^\gamma), \quad (4.15)$$

where $\tilde{P}_{f \rightarrow f\gamma}(z)$ is the real collinear emission part of the fermion splitting function (4.1)

$$\tilde{P}_{f \rightarrow f\gamma}(z) = \frac{1+z^2}{1-z}, \quad (4.16)$$

with the soft region ($z \rightarrow 1$) removed (since it is cut off by the upper boundary $1 - \omega_s^\gamma$). In addition there is the finite soft log from (3.28). Combining the above hard collinear logs with the soft logs and virtual corrections, we recover the universal form seen in [9] $B \rightarrow K\ell\ell$, namely

$$\left[|\mathcal{Z}_B|^2 \Gamma_{B \rightarrow \ell\bar{\nu}(\gamma)} \right]_{\text{hc}}^{\text{S-P}} = \frac{\alpha}{\pi} Q_{\ell_1}^2 \left[|\mathcal{Z}_B|^2 \Gamma_{B \rightarrow \ell\bar{\nu}}^{\text{S-P}} \right]^{(0)} \ln m_\ell \times \left(\left[\frac{3}{2} + 2 \ln \omega_s^\gamma \right]_{\text{real (hard)}} + \left[-1 - 2 \ln \omega_s^\gamma \right]_{\text{real (soft)}} + \left[\frac{3}{2} - 2 \right]_{\text{virt}} \right) = 0, \quad (4.17)$$

where all logs do and must cancel in the fully-inclusive case. Conversely, in the V-A case we get ($\bar{z} \equiv 1 - z$)

$$\left[|\mathcal{Z}_B|^2 \Gamma_{B \rightarrow \ell\bar{\nu}(\gamma)} \right]_{\text{hc}}^{\text{V-A}} = -\frac{m_B \tilde{g}^2 m_\ell^2 Q_{\ell_1}}{16\pi^3} \mathcal{B}_{M^2} \Pi_{f_B}(p_B^2) \ln m_\ell \times \int_{1-r_E}^{1-\omega_s^\gamma} dz \left[Q_{\ell_1} \tilde{P}_{f \rightarrow f\gamma}(z) \mathcal{B}_{M^2} \Pi_{f_B}(p_B^2) + \frac{m_B}{m_+} \bar{z}^2 (V_{\parallel}(z m_B^2) - V_{\perp}(z m_B^2)) \mathcal{Z}_B \right], \quad (4.18)$$

we get besides the splitting function piece (which we could integrate) the form factor parts which truly probes the structure of the B_q -meson! We note that in the soft limit the S-P and the V-A pieces match since the structure of the mesons is not resolved (due to the extra \bar{z}^2 -factor). In that case it is described by the universal formulae [7, 8].

5 Numerics and phenomenology

5.1 Sum rule numerics

The numerical input is given in Tab. 2 in App. A. The sum rule procedure requires two parameters, the continuum threshold s_0 and the Borel parameter M^2 , to be fixed. By the very assumption of the method, semi-global quark hadron duality (e.g. [72]), the threshold s_0 ought to be in between the pole m_B^2 and the onset of the QCD-continuum around $(m_B + 2m_\pi)^2$ (or $(m_B + m_\rho)^2$). If the sum rule was exact the value of the Borel parameter is immaterial and thus the independence thereof is a measure of the quality of the sum rule. In practice the Borel parameter and s_0 values have to be such that the condensate expansion converges (e.g. NLO terms not exceeding 30%) and that the continuum hadronic contributions relative to the B -pole does not exceed 30% [73, 74]. Moreover, we make use of the daughter sum rule (DSR) consistency condition

$$m_B^2 = \frac{\int_{m_+^2}^{s_0} s \rho_{\Pi(\gamma)}(s) e^{-s/M^2} ds}{\int_{m_+^2}^{s_0} \rho_{\Pi(\gamma)}(s) e^{-s/M^2} ds}, \quad (5.1)$$

which must hold in full QCD since $\rho_{\Pi(\gamma)}(s) \propto \delta(s - m_B^2)$, provided s_0 is below the QCD-continuum threshold. Note that to ensure the cancellation of the soft IR divergences between real and virtual, Π and Π^γ must have the same sum rule parameters. On the other hand, the sum rule for the main process Π and the denominator C are not required to have the same values. In certain cases they have to be taken rather different as otherwise the above mentioned criteria are not obeyed e.g. [75]. In practice, since QED is rather small the parameters will be similar to the ones of the f_B sum rule. Following the advertised procedures, we find the following parameters

$$\begin{aligned} \Pi^{(\gamma)}(p_B^2, p_\Phi^2) : \quad & s_0 = 37.2(10) \text{ GeV}^2, \quad M^2 = 7.9(5) \text{ GeV}^2, \\ C(p_B^2, p_\Phi^2) : \quad & s_0 = 36.9(10) \text{ GeV}^2, \quad M^2 = 6.3(5) \text{ GeV}^2. \end{aligned} \quad (5.2)$$

We use the same parameters for all channels $\ell = e, \mu, \tau$ consistent with the relative smallness of the QED-correction. The most relevant input parameter is m_b for which the kinetic scheme [76] has proven to give good convergence in QED-related sum rule physics (e.g. $B \rightarrow \gamma$ form factor [42], the $g_{BB^*(B_1)\gamma}$ coupling [60] and the neutral-charged mass difference [77]). We have found similar patterns and therefore use the kinetic scheme with $m_b^{kin} = 4.53(6) \text{ GeV}$ at $\mu_{kin} = 1 \text{ GeV}$ (with $\overline{\text{MS}}$ -conversion formulae given in [78]). However, in view of that our computation is LO in α_s we vary the m_b -uncertainty by $\delta m_b = \pm 0.2 \text{ GeV}$ thereby accommodating the $\overline{\text{MS}}$ or pole scheme.

The main result reported is the relative QED-correction to the LO decay rate, $\Delta\Gamma_{\text{QED}}$, as a function of the photon energy cut E_γ^{cut}

$$1 + \Delta\Gamma_{\text{QED}}(E_\gamma^{\text{cut}}) \equiv \frac{1}{\Gamma(0)} \left(\Gamma^{B \rightarrow \ell \bar{\nu}} + \Gamma_{E_\gamma < E_\gamma^{\text{cut}}}^{B \rightarrow \ell \bar{\nu} \gamma} \right) + \mathcal{O}(\alpha^2). \quad (5.3)$$

Uncertainties are computed by varying the input parameters, and adding uncertainties in quadrature. It is worthwhile to recall that for structure-dependent corrections, unlike scalar QED, the virtual and the real corrections are separately well-defined. Thus, it makes sense to discuss them separately. The virtual contribution is rather stable showing a $\mathcal{O}(6\text{--}7\%)$ uncertainty. It is mainly due to the m_b -variation for which the uncertainty, when integrated over the s -integral (2.10) from m_b^2 to s_0 , tends to cancel which might be seen as accidental. Instead, taking the absolute value of the uncertainty results in an increase by a factor of two to three. In order to remain on the conservative side, we therefore double the original uncertainty. The virtual structure-dependent corrections are given in Tab. 1 where the hierarchy due to large logs generated by $\ln m_\ell/m_B$ is visible. Numerically the

	τ	μ	e
$\Delta\Gamma_{\text{QED}} _{\text{struc}}^{\text{virtual}}$	+2.9(2)%	+4.6(6)%	+7.8(10)%

Table 1: The virtual structure-dependent QED corrections in $B^- \rightarrow \ell^- \bar{\nu}$ for $\ell = \tau, \mu, e$. The small value of the electron mass causes numerical issues for $m_\ell \lesssim 50m_e$. The extrapolation from m_τ down to $50m_e$ is a straight line in $\ln m_\ell$ from which we infer the actual electron case. This results in the relatively large uncertainty.

$q\ell_1$ -, $b\ell_1$ - and $\Phi\ell_1$ -diagrams are dominant and the $\ln m_\ell$ -terms contribute about 2% and 5%

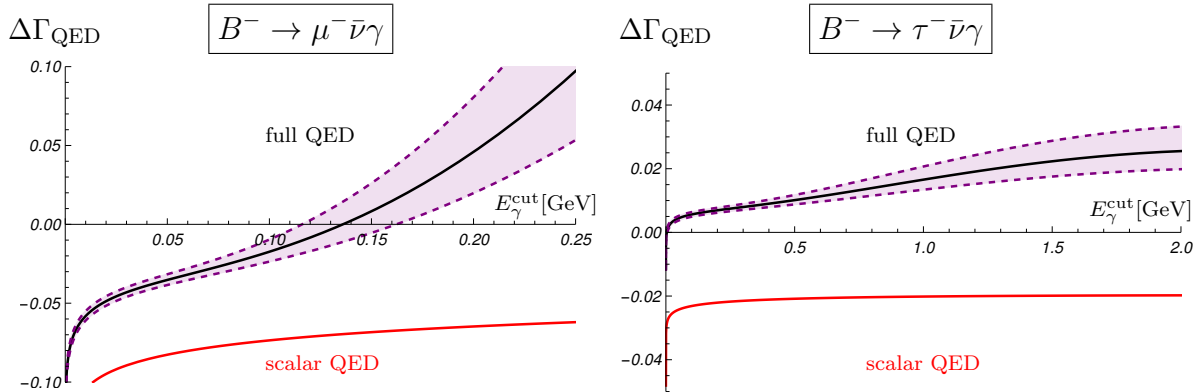


Figure 5: The QED-correction (black line) as a function of the photon energy cut E_γ^{cut} (in GeV), as defined in (5.3). (Left) The muon channel where there is a significant rise due to the lifting of helicity-suppression by the structure-dependent terms. (Right) The tau channel where this effect is less significant due to the large m_τ mass. The error is given by the dashed purple lines and purple bands. For comparison, the red line is the scalar QED result which does not exhibit the same lifting of helicity-suppression. A more detailed version of this plot is given in Fig. 12.

in the muon and electron case respectively. In practice these virtual numbers are extracted from the full real and virtual computation with $V_{\perp,\parallel}^{B \rightarrow \gamma} \rightarrow 0$ (i.e. structure-dependent real radiation) and real and virtual scalar QED subtracted.

Concerning the real radiation, it is relevant to remember that in experiment it is the shape of the final state that enters the fit (folded with detector resolution effects). The shape is taken from a Monte-Carlo simulation (e.g. PHOTOS). Since to-date the latter uses scalar QED it is therefore the shape as compared to scalar QED which is important. In summary not knowing the structure-dependence in effect boils down to an unknown virtual-correction number (as quoted in Tab. (1)) while for the real radiation it is the relative shape in E_γ as compared to the Monte-Carlo which is relevant. We therefore provide the necessary results in the form of Mathematica notebook as an ancillary file to the arXiv version. In the remaining paper we follow the tradition and present the correction in terms of a photon energy cut-off E_γ^{cut} . From a phenomenological viewpoint the crucial feature about the real structure-dependent QED correction is that the helicity-suppression is relieved (by $V_{\perp,\parallel}$ form factor contributions) and becomes exceedingly large when $E_\gamma^{\text{cut}} \gg m_\ell$. Since these form factor uncertainties are sizeable it makes their impact even more noticeable for large E_γ^{cut} .¹² We provide plots for the muon and tau case in Fig. 5; and further breakdowns are shown in Fig. 12.

In the muon case the E_γ^{cut} -interval is restricted to $2m_\mu$ as beyond this the notion of $\Delta\Gamma_{\text{QED}}$ becomes meaningless and one should simply consider $B \rightarrow \ell \bar{\nu} \gamma$ as a decay in its own right. A general feature is that the scalar QED corrections are negative and that the structure-dependent corrections are positive making the overall effect smaller. However,

¹²The form factor uncertainty in $B \rightarrow \gamma$ for maximum recoil is $\mathcal{O}(10\%)$ but at soft-recoil (soft photon) no direct calculation exists and as previously stated the form factor is extrapolated between the pole at $B^*(B_1)$ in the vector and axial channel and thus the uncertainty largely depends on the input of the pole-residue. The latter is computed from a double dispersion sum rule [60] whose accuracy cannot match the single dispersion sum rule [42] for many reasons.

we re-emphasise that since the Monte-Carlo programs to date are based on scalar QED in those channels, knowing the corrections thereto is of importance. We observe:

Muon case: the real structure-dependent corrections exceed the virtual structure-dependent corrections for $E_\gamma^{\text{cut}} > 0.175(31)$ GeV. It is also observed that the QED-correction changes sign for $E_\gamma^{\text{cut}} = 0.136(23)$ GeV. Note that $E_\gamma \approx 0.2$ GeV is a relevant range in view of a typical $K\mu\mu$ -distribution for the LHCb-experiment.

Tau case: the real radiation is less important due to the large τ mass. The overall QED-correction is positive and increases slowly to $+2.60(69)\%$ at the endpoint $E_\gamma^{\text{cut}} = \frac{m_B}{2}(1 - (\frac{m_\tau}{m_B})^2)$.

The plots in Fig. 6 give the real differential branching ratio. Schematically we divide the rate into three characteristic terms

$$\frac{dB(B \rightarrow \ell\bar{\nu}\gamma)}{dE_\gamma} \propto c_1 f_B^2 \frac{m_\ell^2}{E_\gamma} + c_2 f_B \frac{m_\ell^2 E_\gamma^2}{m_B^2} (V_\perp - V_\parallel) \ln m_\ell + c_3 E_\gamma^3 \left(1 - \frac{2E_\gamma}{m_B}\right) (V_\perp^2 + V_\parallel^2) + \dots ,$$

where $c_{1,2,3} = \mathcal{O}(G_F^2 m_\ell^0)$ are known coefficients. These three terms may be associated with three photon energy regions. The first term dominates for ultrasoft photons and in Fig. 6 the $\frac{1}{E_\gamma}$ behaviour is clearly visible in the μ -case but less so for the τ -case since $m_\tau \gg m_\mu$. For soft photons, the proximity of the $B^{*(1)}$ pole enhances the contribution of the second (structure-dependent) term and other similar terms. Finally for non-soft photons, the rate is completely dominated by structure-dependent effects, given in the third term. This highlights the importance of the form factors in the non-ultrasoft region. As the latter are largely determined by the pole residues, as has been emphasised in [79],

$$V_{\perp(\parallel)}^V = \frac{r_{\perp(\parallel)}^V}{1 - q^2/m_{B^{*(1)}}^2} , \quad r_{\perp(\parallel)}^V = \frac{m_B}{m_{B^{*(1)}}} f_{B^{*(1)}} g_{BB^{*(1)}\gamma} , \quad (5.4)$$

it is worthwhile to briefly discuss them. We note that the values in [79], resulting from averaging a few models, are qualitatively different

$$\begin{aligned} r_\perp^V|_{[60]} &\approx -0.30(4) , & r_\parallel^V|_{[60]} &\approx -0.16(3) , & r_\perp^V/r_\parallel^V &\approx 1.9 , \\ r_\perp^V|_{[79]} &\approx -0.24(4) , & r_\parallel^V|_{[79]} &\approx -0.20(5) , & r_\perp^V/r_\parallel^V &\approx 1.2 , \end{aligned} \quad (5.5)$$

in their ratio and as such will give rise to qualitatively different rates (or Dalitz plots).

Further plots of the double differential real rate in E_γ - $\cos(\theta)$ and Dalitz-variables as well as comments on real versus virtual structure-dependence are given in App. A.2.

5.2 Outlook on phenomenology

Let us turn to the relevance for experimental searches. The branching fraction of the leptonic decay without photons and neglecting the neutrino mass is given by

$$\mathcal{B}(B^- \rightarrow \ell^- \bar{\nu}) = \frac{G_F^2 m_B}{8\pi} m_\ell^2 \left(1 - \frac{m_\ell^2}{m_B^2}\right)^2 f_B^2 |V_{ub}|^2 \tau_B , \quad (5.6)$$

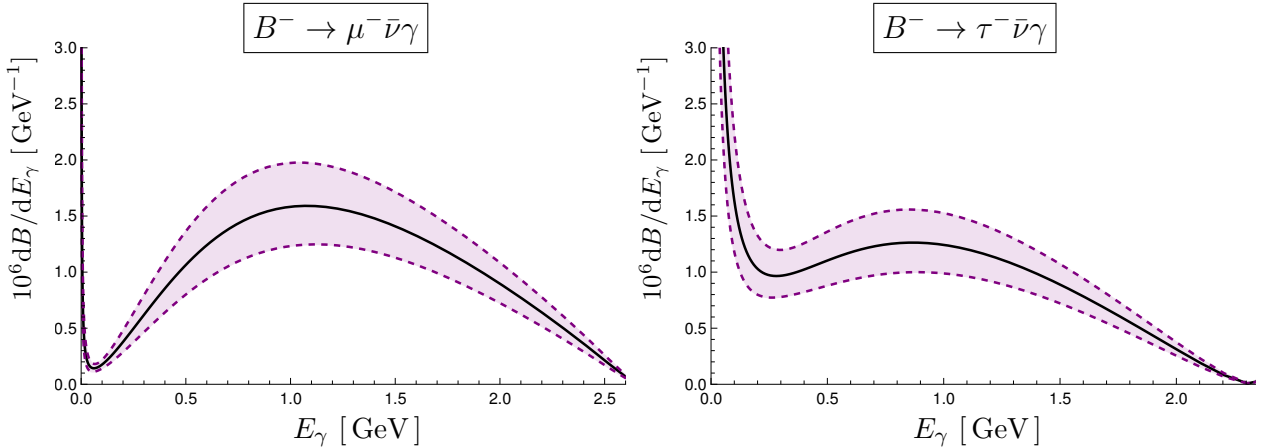


Figure 6: The differential branching ratio $10^6 dB(B \rightarrow \ell \bar{\nu} \gamma) / dE_\gamma$ for $\ell = \mu$ (Left) and $\ell = \tau$ (Right) with the uncertainties in purple. Here there is also the uncertainty due to the CKM matrix element V_{ub} .

where $G_F = 1.166 \times 10^{-5} \text{ GeV}^{-2}$ is the Fermi constant, $\tau_B = 1.638(4) \times 10^{-12} \text{ s}$ the B^+ lifetime, $|V_{ub}|$ a CKM matrix element and f_B the B -meson decay constant, $\langle 0 | \bar{q} \gamma_\mu \gamma_5 b | B(p) \rangle = i f_B p_\mu$. The SM predictions are (e.g. [80])

$$\mathcal{B}(B \rightarrow e \bar{\nu}) \approx 8.1(6) \cdot 10^{-12}, \quad \mathcal{B}(B \rightarrow \mu \bar{\nu}) \approx 3.5(3) \cdot 10^{-7}, \quad \mathcal{B}(B \rightarrow \tau \bar{\nu}) \approx 7.7(6) \cdot 10^{-5}.$$

The main unknowns in (5.6) are $|V_{ub}|$ and f_B of which the latter is directly calculable by non-perturbative methods such as lattice QCD and its current uncertainty is already below a percent [81]. The remaining uncertainty is due to $|V_{ub}|$ and is related to the $|V_{ub}|$ - $|V_{cb}|$ tension between inclusive/exclusive-determinations as well as the CKM triangle fit (e.g. [82]). The τ -rate has been measured at the B -factories Belle [83, 84] and BaBar [85, 86] and its PDG average $\mathcal{B}(B \rightarrow \tau \bar{\nu}) = 1.09(24) \cdot 10^{-4}$ [87] shows some tension with the prediction. However, uncertainties are too large for the QED-correction computed in this paper to be relevant unlike in future measurement (as discussed below). For the μ - and e -rate only confidence limits exist. Whereas for the electron the SM rate is beyond the Belle II capabilities the μ -rate is expected to be measured with 6 ab^{-1} at the 5σ confidence level [80]. At 50 ab^{-1} the estimated uncertainties, which are statistically dominated, are [80]

$$\Delta \mathcal{B}(B \rightarrow \mu \bar{\nu})|_{@50 \text{ ab}^{-1}} \approx 7\%, \quad \Delta \mathcal{B}(B \rightarrow \tau \bar{\nu})|_{@50 \text{ ab}^{-1}} \approx (6, 5)\%. \quad (5.7)$$

The two numbers in the τ case are for a hadronic and a semileptonic tag respectively and could be averaged as they come from different data sets. The fact that the μ -channel is competitive despite lower statistics is owed to it being a clean final state without decaying hadronically. We conclude that, in view of the uncertainties in (5.7), our predictions of 5% and 3% virtual structure-dependent QED-corrections are certainly relevant. The relevance of the real radiation depends on two matters. Firstly, how inclusive the measurement is, for which the value of the photon energy cut E_γ^{cut} is indicative (cf. Fig. 12). Second and as emphasised previously, how different the shape of the real radiation is with respect to

scalar QED (and this is used to inform or compare against QED Monte-Carlo programs). In view of Fig. 12 one has to conclude that it is rather relevant in the μ -channel.

In view of the $|V_{ub}|$ -uncertainty it is attractive to consider ratios [80, 88]

$$R_{\text{pl}} = \frac{\mathcal{B}(B^- \rightarrow \tau^- \bar{\nu})}{\mathcal{B}(B^- \rightarrow \mu^- \bar{\nu})} \Big|_{@50\text{ab}^{-1}} = 222(26) ,$$

$$R_{\text{ps}} = \frac{\tau_{B^0}}{\tau_{B^-}} \frac{\mathcal{B}(B^- \rightarrow \tau^- \bar{\nu})}{\mathcal{B}(B^0 \rightarrow \pi^+(e, \mu)^- \nu)} \Big|_{@50\text{ab}^{-1}} = 0.54(4) , \quad (5.8)$$

where this quantity drops out and the structure-dependent QED-corrections are even more relevant. For R_{pl} , f_B equally drops and QED probing the hadrons is then the sole hadronic remnant. The experimental uncertainties, shown in (5.8) for 50ab^{-1} , are however large, since the systematics are of an entirely different origin and thus add. Whereas this method currently seems a viable alternative, it cannot compete once the $|V_{ub}|$ -uncertainty drops significantly. However, in that case it can still serve as a cross-check of the actual $|V_{ub}|$ -determination itself.

6 Conclusions and summary

In this work we have applied the framework of gauge invariant interpolating operators, proposed in [14], in the concrete setting of leptonic decays. As all universal IR logs are reproduced this constitutes a strong consistency check of the method. We show that the $B^- \rightarrow \ell^- \bar{\nu}$ mode with S-P (Yukawa-type) interactions exhibit no structure-dependent hard collinear logs in accordance with the entirely general arguments based on gauge invariance and the KLN-theorem [9]. However, the Standard Model leptonic decay is an exception as the chiral suppression circumvents the assumption in [9]. Hence, these logs can and do arise as confirmed by our explicit results (and reasoned in [13]).

To the best of our knowledge our work provides the first computation of structure-dependent QED-corrections in $B^- \rightarrow \ell^- \bar{\nu}$ (the SCET analysis [33] awaits a further study). Our main results are summarised in Fig. 5 (and in more detail in Fig. 12), showing virtual and real structure-dependent QED-corrections separately on top of the point-like approximation. The structure-dependent virtual corrections are +4.6(6)% and +2.9(2)% in the μ - and τ -case. Uncertainties due to the real radiation are sizeable. In practice, for the real radiation, what is important is not its size but rather its shape since that is what enters modern experimental analyses. As the shape is found to be qualitatively different from scalar QED, used in current Monte-Carlo programs, its inclusion is also of relevance. (We append a Mathematica notebook to the arXiv version for this purpose.) Partly for traditional reasons we additionally provide plots of the relative QED-corrections as a function of the photon energy cut-off E_γ^{cut} . In the μ -channel real and virtual structure-dependent corrections are comparable for $E_\gamma^{\text{cut}}|_\mu \approx 0.18(3)$ GeV, whereas in the τ -channel the real radiation is never comparable even when fully inclusive. The origin of this qualitative difference is that the chirality suppression is effectively not there in the τ -case.

The actual phenomenological importance is discussed in Sec. 5.2. The size of the corrections are certainly relevant in comparison to the $B^- \rightarrow \ell^- \bar{\nu}$ theory uncertainty which

itself is dominated by $|V_{ub}|$ since the B -meson decay constant f_B is known to percent-accuracy. The $|V_{ub}|$ -dependence leads to an interplay with the $|V_{ub}|-|V_{cb}|$ puzzle whose resolution is important in many ways (e.g. in the prediction of rare B decays). Our framework equally applies to D decays (and possibly K decays) to which we might return in a future work.

Acknowledgments

RZ is supported by an STFC Consolidated Grant, ST/P0000630/1. We are grateful to Will Barter and Franz Muheim for discussions. In addition we acknowledge Saad Nabeebaccus for useful discussions and comments on the manuscript. Many loop computations are performed with the FEYN CALC package [89, 90] and PACKAGE-X [91].

A Conventions, inputs and plots

We work with the QED covariant derivative

$$D_\mu = \partial_\mu + ies_e Q_f A_\mu, \quad (\text{A.1})$$

with $e > 0$ (and $s_e = \pm 1$ are frequently chosen conventions), $Q_\Phi = Q_{\ell_1} = -1$, $Q_b = -1/3$, $Q_u = 2/3$ and we take $\epsilon_{0123} = +1$.¹³ The particle masses, lifetimes and other input parameters used for our calculation are summarised in Tab. 2.

For the slicing procedure, we take $\omega_s = \omega_s^\gamma$ at $s = m_B^2$, and enforce the hierarchy $\omega_c/\omega_s \ll 1$ as far as possible. We take $\omega_s^{(e)} = 10^{-3}$, $\omega_s^{(e)} = 100 \cdot \omega_c^{(e)}$, while the heavier muon channel constrains us to take $\omega_s^{(\mu)} = 5 \cdot 10^{-3}$ and $\omega_s^{(\mu)} = 50 \cdot \omega_c^{(\mu)}$. No slicing is performed for the τ channel. These choices give good stability.

A.1 Condensate contributions

This appendix details the contribution of the quark condensate $\langle \bar{q}q \rangle$ -diagrams shown in Figs. 7, 8 and 9.

On the one hand these diagrams are simpler as they are only one-loop, however the cuts are more involved. Consider the virtual diagrams first. For the condensates we work in the $m_q = 0$ approximation which is well justified as light quark mass effects are small in this case. The LO results are

$$\begin{aligned} \text{Im} \Pi_{\langle \bar{q}q \rangle}^{(0)} &= -\pi m_+ g_{\text{eff}} \langle \bar{q}q \rangle m_\ell \bar{u} \Gamma v \delta^+(p_B^2 - m_b^2), \\ \text{Im} C_{\langle \bar{q}q \rangle}^{(0)} &= -\pi m_+^2 m_b \langle \bar{q}q \rangle \delta^+(p_B^2 - m_b^2). \end{aligned} \quad (\text{A.2})$$

Due to the presence of the delta functions, it is often easier to give results after Borel transformation. Gauge invariance of the 1PI diagrams works out similarly to (3.12)

$$\text{Im} \Pi_{\langle \bar{q}q \rangle}^{(2)}|_{1-\xi} = g_{\text{eff}} m_+ e^2 \langle \bar{q}q \rangle (Q_{\ell_1} - Q_b + Q_q) (Q_\Phi - Q_b + Q_q) \frac{m_\ell \bar{u} \Gamma v}{32\pi^2 p_B^2}$$

¹³Note that the notation used in [9] with charges s.t. $\sum \hat{Q}_i = 0$ is not particularly useful anymore since there is now more than one vertex and the quark charges would take on different roles in the two vertices (ingoing charges in \mathcal{L}_w versus outgoing in \mathcal{J}_B).

Boson masses [87]		
m_{B^-}	M_W	M_Z
5.279 GeV	80.377 GeV	91.19 GeV
Lepton masses [87]		
m_τ	m_μ	m_e
1.777 GeV	105.7 MeV	0.511 MeV
Quark masses [87]		
$m_b^{kin} _{1\text{GeV}}$	$\bar{m}_u _{2\text{GeV}}$	
4.53(6) GeV	$2.16^{+0.49}_{-0.26}$ MeV	
Miscellaneous [87]		
τ_{B^-}	G_F	α^{-1}
$1.638(4) \times 10^{-12}$ s	1.166×10^{-5} GeV $^{-2}$	137.036
$\langle \bar{q}q \rangle _{2\text{GeV}}$ [92]	$ V_{ub} $	
$-(269(2) \text{ MeV})^3$	$3.82(20) \times 10^{-3}$	

Table 2: Summary of input parameters. Uncertainties in the meson masses are negligible. We set the renormalisation scale $\mu = m_b$, although the scale dependence upon varying $\mu^2 \rightarrow \{0.5, 2\}\mu^2$ is negligible since it is $\mathcal{O}(\alpha^2)$ and below numerical precision.

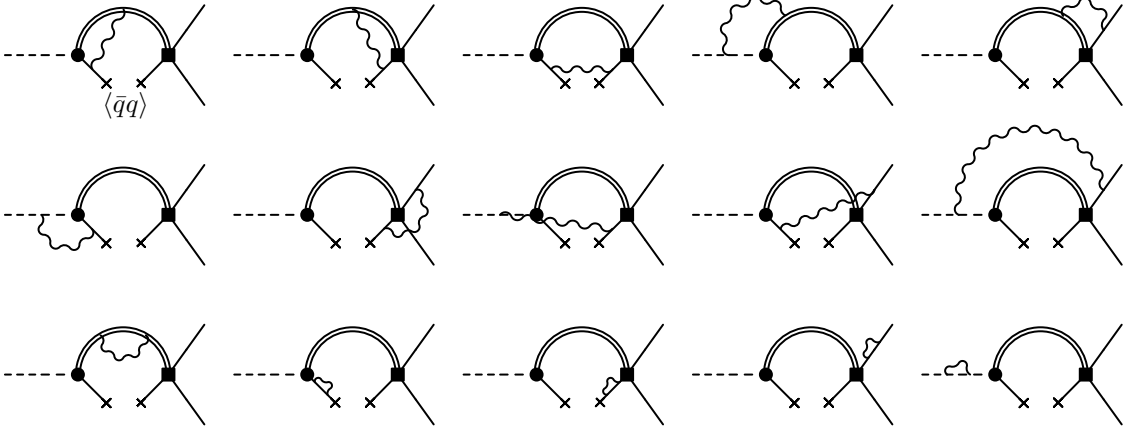


Figure 7: Virtual quark condensate diagrams contributing to $\Pi_{\langle \bar{q}q \rangle}^{(2)}$ in (2.4) (the main process). The two crosses denote the quark condensate $\langle \bar{q}q \rangle$.

$$\times (B_0(p_B^2, 0, m_b^2) - (m_b^2 + p_B^2)C_0(0, p_B^2, p_B^2, 0, 0, m_b^2)) = 0, \quad (\text{A.3})$$

while for the denominator

$$\text{Im } C_{\langle \bar{q}q \rangle}^{(2)}|_{1-\xi} = -\frac{m_+^2 e^2}{16\pi^2} m_b \langle \bar{q}q \rangle (Q_\Phi - Q_b + Q_q)^2 C_0(0, p_B^2, p_B^2, 0, 0, m_b^2) = 0. \quad (\text{A.4})$$

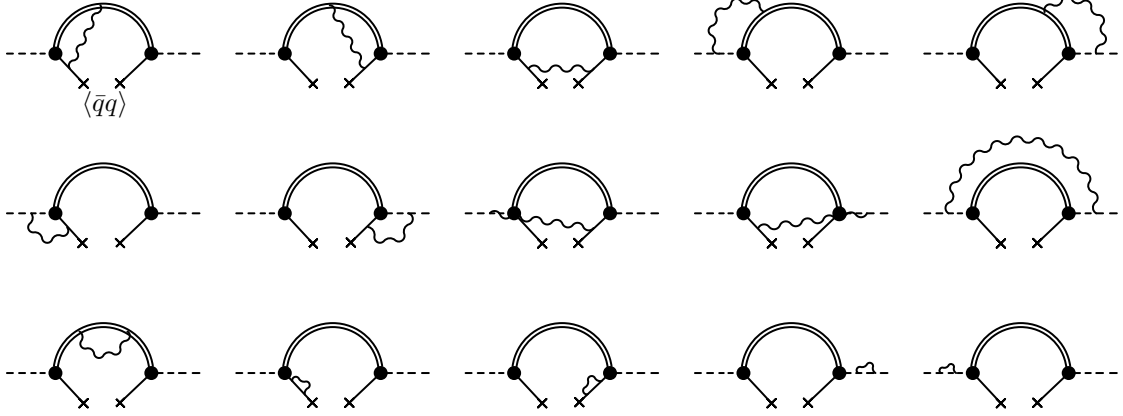


Figure 8: Quark condensate diagrams contributing to $C_{\langle\bar{q}q\rangle}^{(2)}$ (2.13), that is $|\mathcal{Z}_B|^2$ (2.14) (the denominator).

Here B_0 and C_0 are the usual Passarino-Veltman functions with FEYNCalc normalisation $(2\pi\mu)^{2\epsilon} \int \frac{d^d k}{i\pi^2}$. In the condensates in general, and in this C_0 in particular, we encounter non-logarithmic (power) singularities at the endpoint $p_B^2 \rightarrow m_b^2$. One can see this by using the derivative trick of (3.6)

$$\begin{aligned} \text{Im } C_0(0, p_B^2, p_B^2, 0, 0, m_b^2) &= \frac{(2\pi\mu)^{2\epsilon}}{i\pi^2} \lim_{N^2 \rightarrow 0} \frac{d}{dN^2} \text{Im} \int \frac{d^d k}{((p_B - k)^2 - m_b^2)(k^2 - N^2)} \\ &= -\pi(1 + \epsilon(-\gamma_E + \ln 4\pi\mu^2)) \frac{p_B^2 + m_b^2}{(p_B^2)^{1-\epsilon}(p_B^2 - m_b^2)^{1+2\epsilon}}, \end{aligned} \quad (\text{A.5})$$

a form seen in [93]. The divergence as $p_B^2 \rightarrow m_b^2$ is of the IR-type, regulated by $\epsilon < 0$. On the other hand the $(p_B^2)^{1-\epsilon}$ part regulates the UV ($\epsilon > 0$) as $p_B^2 \rightarrow \infty$ (after Borel transformation all UV divergences disappear since they are local). The IR divergence is manifest after the Borel transform

$$\mathcal{B}_{M^2} C_0 = e^{\frac{m_B^2 - m_b^2}{M^2}} \left(\frac{1}{\hat{\epsilon}_{\text{IR}}} + \ln \frac{s_0 \mu^2}{(s_0 - m_b^2)^2} - \int_{m_b^2}^{s_0} \frac{s + m_b^2}{s(s - m_b^2)} \left(e^{\frac{m_b^2 - s}{M^2}} - 1 \right) ds \right), \quad (\text{A.6})$$

where we have used a subtraction method in order to separate out the divergent part of the integral.

The discontinuities are obtained from the standard cutting rules, though the soft slicing takes a different form for the red cuts. As there is one less loop, compared to the perturbative contribution, the red cuts resemble a $1 \rightarrow 2$ real decay and thus the photon energy is fixed. The $\delta^+(p_B^2 - m_b^2) \ln \Delta E_s$ term, generated from the soft region, cancels with a $\theta(p_B^2 - m_b^2 - 2m_b \Delta E_s)/(p_B^2 - m_b^2)$ only after Borel transformation, with the $\ln \Delta E_s$ dependence arising from an incomplete Gamma function. As before, for all diagrams that do not involve a q quark leg, the soft divergence cancels between red and blue cuts. The denominator $\Phi\Phi$ - and numerator $\Phi\ell_1$ -diagrams (which only have red cuts) give physical soft divergences that cancel with the self-energies (denominator) and real radiation (nu-

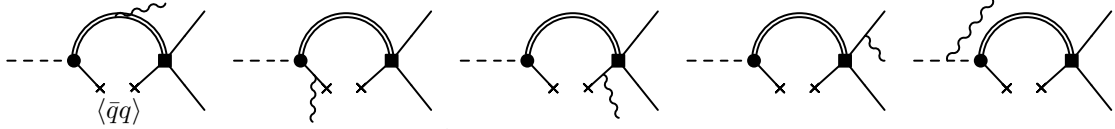


Figure 9: Quark condensate diagrams contributing to $\Pi_{\langle \bar{q}q \rangle}^\gamma$ in (2.4) (i.e. the radiative or real emission part). We stress again that the diagrams where the photon connects to the quarks are subsumed by using external form factors [42].

merator) as in the perturbative calculation. Indeed we recover the universal soft form for the numerator with $\text{Im } \Pi_{\perp}^{(0)} \rightarrow \text{Im } \Pi_{\langle \bar{q}q \rangle}^{(0)}$.

The diagrams where the photon connects to a condensate q -quark leg are the ones that contribute endpoint IR divergences. Applying charge conservation, the sum of these diagrams is proportional to Q_q^2 . These IR divergences cancel against q -quark self energies $\sim Q_q^2 (\frac{1}{\epsilon_{UV}} - \frac{1}{\epsilon_{IR}})$ (which formally vanish in DR if $\epsilon_{UV/IR}$ is not paid attention to). Now as UV divergences, these terms are removed by the same renormalisations as for the perturbative diagrams serving as a sanity check of the procedure.

In the numerator a similar slicing procedure can be performed for the collinear logs though now the photon energy is fixed, forcing $z \rightarrow \delta_H = m_b^2/p_B^2$. There are two $q \ell_1$ -diagrams (one from each condensate leg) which must be handled with care.

The real condensate contributions are simpler with $\text{Im } \Pi_{f_B}^{\langle \bar{q}q \rangle} = -\pi \langle \bar{q}q \rangle \delta^+(p_B^2 - m_b^2)$ because all other condensate contributions are contained in the form factors $V_{\parallel, \perp}$ taken from [42].

A.2 More detailed plots

In this appendix, we present plots with further details. In Fig. 10, we give the normalised Dalitz plot, that is $\frac{1}{\Gamma^{(0)}} \frac{d^2\Gamma}{dx dy}$, the double differential decay rate normalised to the LO rate (this type of plot has been shown in [79] for a pole model of form factors). Alternatively in Fig. 11, the double differential rate is given as $\frac{1}{\Gamma^{(0)}} \frac{d^2\Gamma}{dx d \cos \theta}$. Here, the lifting of the helicity-suppression for hard photons is obvious in the muon case. For soft photons, there is a small enhancement visible near $\cos \theta = 1$ which is the collinear region.

In Fig. 12 we give the full QED-correction, $\Delta\Gamma_{\text{QED}}$, of Fig. 5 (black line) and with real structure-dependent form factors $V_{\perp, \parallel}$ set to zero (blue line), and scalar QED is indicated in red as before. The difference between the red and blue (dashed) line therefore corresponds to the virtual structure-dependent QED-correction (estimated to be +4.6% and +2.9% for μ and τ respectively). Conversely, the difference between the black line and the blue line corresponds to the real structure-dependent contribution.¹⁴

¹⁴Note that it is important to use the same scheme, $\overline{\text{MS}}$ in DR in our case, for real and virtual contributions to make the separation well-defined. This applies to scalar QED as there are $1/\epsilon_{\text{IR}}$ -terms and the scheme affects the finite parts, temporarily.

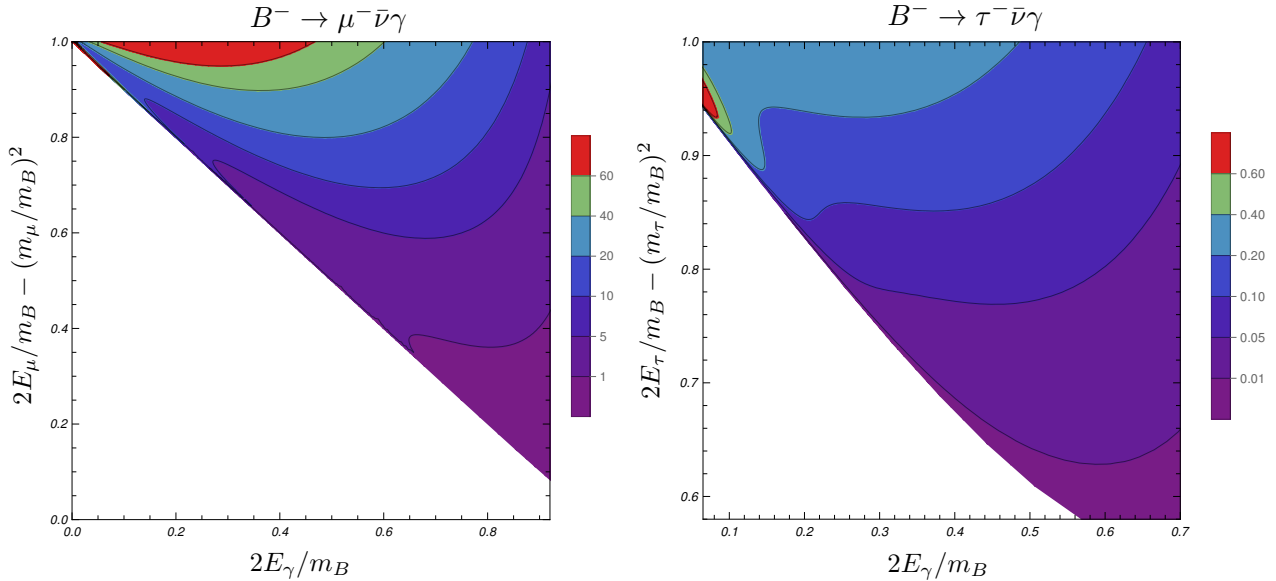


Figure 10: The Dalitz plot $\frac{1}{\Gamma^{(0)}} \frac{d^2\Gamma}{dx dy}$ for muons (Left) and taus (Right). The contours show the enhancement from the non-radiative rate. For example on the left the red contour shows where the number of radiative events is 60 times the number for the non-radiative decay. There are peaks in the soft regions, and where the structure-dependent contributions dominate.

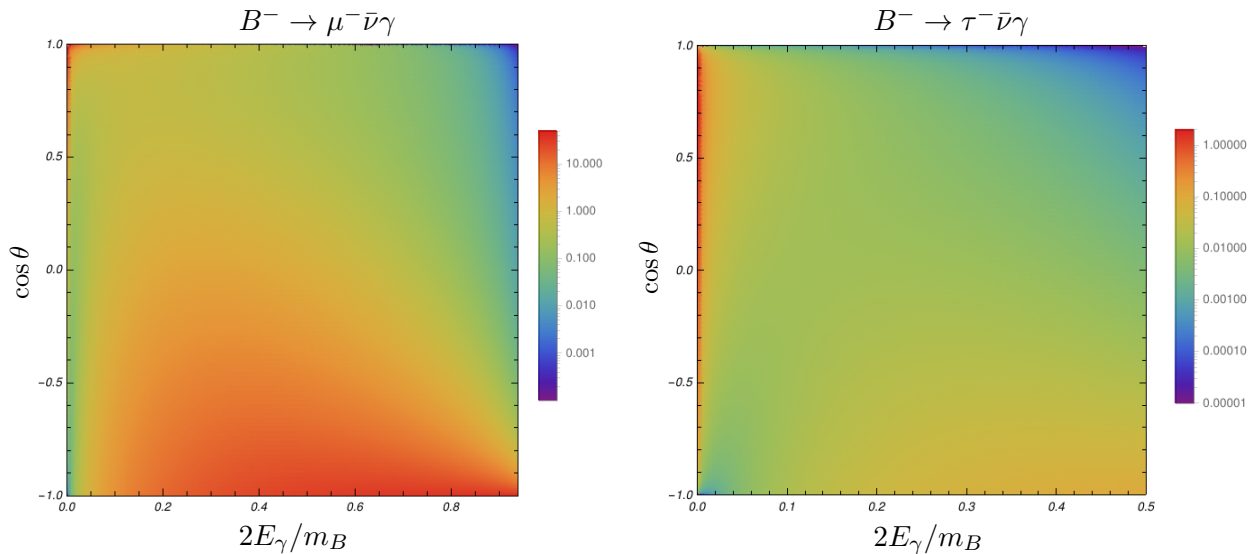


Figure 11: The double differential rate $\frac{1}{\Gamma^{(0)}} \frac{d^2\Gamma}{dx d \cos \theta}$ for muons (Left) and taus (Right). The angle θ is the angle between the photon and the lepton in the B -meson rest frame. Note the colourbar has a different scale for the two channels.

B Further aspects

B.1 On the necessity of all cuts

It is interesting to contrast our approach with the one taken in the calculation of $B \rightarrow \gamma$ form factors $V_{\parallel,\perp}$ (e.g. [42]). We may consider the situation where we compute the real

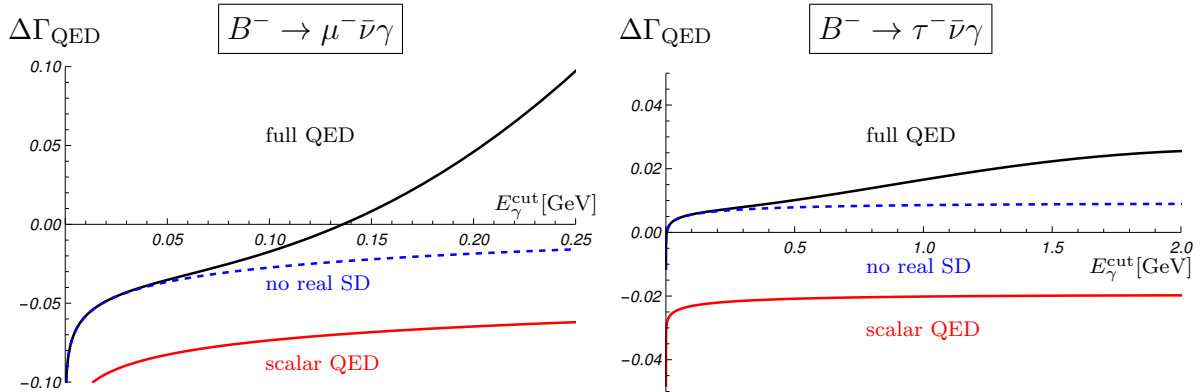


Figure 12: The structure-dependent (SD) contributions to $\Delta\Gamma_{\text{QED}}$, cf. Fig. 5 for muons (Left) and taus (Right). As well as the full result (black) and the scalar QED result (red), we give our calculation having set the real form factors $V_{\parallel,\perp}$ to zero (blue, dashed). This allows us to gauge the contribution of the real and virtual structure-dependent effects.

emission completely within our formalism.¹⁵ For the real diagrams, both red (where we cut *after* the photon is radiated) and blue (where we cut *before*), would have to be taken whereas in [42] only the blue cuts are considered. How can this be reconciled?

As discussed in [14] (Appendix A.1) and in the main text, the resolution is that the red cuts do not contribute for hard photons ($q^2 \gtrsim 14 \text{ GeV}^2$) considered in [42]. To illustrate the differences consider the real amplitude without structure-dependence, ignoring lepton radiation, it reads

$$\begin{aligned}
 (\Pi^\gamma)^\rho = & -\tilde{g}Q_\Phi \frac{p_\Phi^\rho}{p_\Phi \cdot k} \Pi_{f_B}(q^2) m_\ell \bar{u} \Gamma v + \\
 & \tilde{g}Q_\Phi \bar{u} \Gamma_\mu v \left(\frac{\Pi_{f_B}(q^2) - \Pi_{f_B}(p_B^2)}{k \cdot p_B} (p_B)^\rho (p_B)^\mu - \Pi_{f_B}(q^2) g^{\rho\mu} \right) + \dots \quad (\text{B.1})
 \end{aligned}$$

The first term comes from the Φ -diagram with the second line being the contact terms arising from the quark radiation. Taking red cuts is equivalent to cutting $\Pi_{f_B}(q^2)$ while the blue cuts correspond to cutting $\Pi_{f_B}(p_B^2)$. As we take all cuts in our formalism the contact terms are $\mathcal{O}(E_\gamma^0)$ with the Φ -diagram providing the correct Low behaviour as $q^2 \rightarrow p_B^2$. Conversely, if one treats q^2 as a separate variable and only cuts in p_B^2 (blue cuts only) then $(\Pi_{f_B}(q^2) - \Pi_{f_B}(p_B^2))/(k \cdot p_B) \xrightarrow{\text{cut}} -\text{Im} \Pi_{f_B}(p_B^2)/(k \cdot p_B)$ which is the analogy of the Φ term. This resolves the apparent contradiction. Note that in the $B \rightarrow \gamma$ formalism gauge variant operators are used (no Φ field) which is acceptable for hard photons as the Φ -diagram (emission from the Φ) only have red cuts. Our approach is more general as both hard and soft photons can be treated.

On the virtual side taking all the cuts is non-negotiable as it is required for the cancellation of non-physical IR divergences. For example diagrams which connect to the q -quark leg generate collinear $\ln m_q$ terms individually in both the red and blue cuts, but these

¹⁵This would correspond to computing the form factors $V_{\perp,\parallel}$ explicitly in the soft photon-region. As lamented before, this is not easily possible because of the $B^{*,1}$ -poles but it is still interesting to reflect on the cuts which is the aim of this section.

cancel between the cuts

$$\begin{aligned}\text{Im } \Pi_{\text{blue}}^{(2)}|_{\ln m_q} &= +\frac{\alpha}{\pi} Q_q \left(Q_{\ell_1} + Q_{\Phi} - 2Q_b + \frac{5}{2} Q_q \right) \text{Im } \Pi_{m_q \rightarrow 0}^{(0)}, \\ \text{Im } \Pi_{\text{red}}^{(2)}|_{\ln m_q} &= -\frac{\alpha}{\pi} Q_q \left(Q_{\ell_1} + Q_{\Phi} - 2Q_b + \frac{5}{2} Q_q \right) \text{Im } \Pi_{m_q \rightarrow 0}^{(0)}.\end{aligned}\quad (\text{B.2})$$

As particles are put on-shell when cut, individual cuts also generate soft divergences. For a given diagram in the soft limit, taking the blue and red cuts together, the result is proportional to $\int_k \left(\frac{1}{k^2} + 2\pi i \delta^+(k^2) \right) f$, where f is the rest of the integrand (and diagram-dependent). The $1/k^2$ comes from the blue cut while the delta function arises from the red cut. As f in general contains no poles in the lower half plane, one may evaluate the k^0 integral by the residue theorem. The blue cut picks up the only pole at $k^0 = |\mathbf{k}| - i0$ which puts the photon on-shell and exactly cancels the effect of the $\delta^+(k^2)$. Thus the unphysical soft divergences cancel between blue and red cuts.

B.2 Toy model

The methodology of this paper was first tested in a simple toy model where the quark loop is replaced by a scalar B propagator as shown in Fig. 4. Reassuringly, all features such as gauge invariance, the universal soft logs and the universal hard-collinear logs (S-P case) are reproduced. It is interesting to look at the hard-collinear logs. Specifically, for the virtual 1PI diagrams we find

$$\begin{aligned}\Pi_{\text{Toy,S-P}}^{(2),1\text{PI}}|_{\ln m_\ell} &= -\frac{\alpha}{\pi} \Pi_{\text{Toy,S-P}}^{(0)} \times \ln m_\ell, \\ \Pi_{\text{Toy,V-A}}^{(2),1\text{PI}}|_{\ln m_\ell} &= \frac{\alpha}{2\pi} \left(1 + \mathcal{O}(l_2 \cdot r) \right) \Pi_{\text{Toy,V-A}}^{(0)} \times \ln m_\ell.\end{aligned}\quad (\text{B.3})$$

As expected in the S-P case, scalar QED is recovered straightforwardly. To recover scalar QED in the V-A case equation (B.3) instructs us to take the (sensible) choice $l_2 \cdot r = 0$. This extra freedom in the V-A case is a consequence of helicity-suppression and offers a hint at structure-dependent hard-collinear logs. For the real radiation, discarding the extra

Contribution	S-P	V-A
Real	$-1 + r_E(2 - \frac{1}{2}r_E)$	$-1 + r_E(2 - \frac{1}{2}r_E)$
Virtual (1PI)	-2	1
Virtual (Z)	$\frac{3}{2}$	$\frac{3}{2}$

Table 3: The table shows the coefficients of $\frac{\alpha}{\pi} \Gamma^0 \ln(m_\ell)$ broken up into the real, virtual (1PI) and virtual (renormalisation) $\mathcal{O}(\alpha)$ contributions in scalar QED. The overall collinear logs are given by summing the columns. In the fully inclusive case ($r_E \equiv 2E_\gamma^{\text{cut}}/m_B \rightarrow 1$) the S-P $\ln(m_\ell)$ cancel as expected while there are $3 m_\ell^2 \log(m_\ell)$ left over in the V-A. Note $-\frac{3}{2} + r_E(2 - \frac{1}{2}r_E)$ is just the splitting function in disguise, cf. (4.3).

structures involving r , scalar QED is recovered exactly. For convenience, an overview of the scalar QED logs is give in Tab. 3 (cf. also [13]). Note that the S-P and the V-A real rates are fully identical in scalar QED as a consequence of the equation of motion. This is reflected in the identical real splitting function in the table (cf. caption of Tab. 3).

References

- [1] V. Chung, “Infrared Divergence in Quantum Electrodynamics,” *Phys. Rev.* **140** (1965) B1110–B1122.
- [2] T. W. B. Kibble, “Coherent soft-photon states and infrared divergences. ii. mass-shell singularities of green’s functions,” *Phys. Rev.* **173** (1968) 1527–1535.
- [3] T. W. B. Kibble, “Coherent soft-photon states and infrared divergences. iii. asymptotic states and reduction formulas,” *Phys. Rev.* **174** (1968) 1882–1901.
- [4] T. W. B. Kibble, “Coherent soft-photon states and infrared divergences. iv. the scattering operator,” *Phys. Rev.* **175** (1968) 1624–1640.
- [5] P. P. Kulish and L. D. Faddeev, “Asymptotic conditions and infrared divergences in quantum electrodynamics,” *Theor. Math. Phys.* **4** (1970) 745.
- [6] F. Bloch and A. Nordsieck, “Note on the Radiation Field of the electron,” *Phys. Rev.* **52** (1937) 54–59.
- [7] D. R. Yennie, S. C. Frautschi, and H. Suura, “The infrared divergence phenomena and high-energy processes,” *Annals Phys.* **13** (1961) 379–452.
- [8] S. Weinberg, “Infrared photons and gravitons,” *Phys. Rev.* **140** (1965) B516–B524.
- [9] G. Isidori, S. Nabeebaccus, and R. Zwicky, “QED corrections in $\bar{B} \rightarrow \bar{K} \ell^+ \ell^-$ at the double-differential level,” *JHEP* **12** (2020) 104, [arXiv:2009.00929 \[hep-ph\]](#).
- [10] G. Isidori, D. Lancierini, S. Nabeebaccus, and R. Zwicky, “QED in $\bar{B} \rightarrow \bar{K} \ell^+ \ell^-$ LFU ratios: Theory versus Experiment, a Monte Carlo Study,” [arXiv:2205.08635 \[hep-ph\]](#).
- [11] T. Kinoshita, “Mass singularities of Feynman amplitudes,” *J. Math. Phys.* **3** (1962) 650–677.
- [12] T. D. Lee and M. Nauenberg, “Degenerate Systems and Mass Singularities,” *Phys. Rev.* **133** (1964) B1549–B1562.
- [13] R. Zwicky, “QED-Corrections to Weak Decays,” *Symmetry* **13** no. 11, (2021) 2036, [arXiv:2205.06194 \[hep-ph\]](#).
- [14] S. Nabeebaccus and R. Zwicky, “Resolving charged hadrons in QED — gauge invariant interpolating operators,” *JHEP* **11** (2022) 101, [arXiv:2209.06925 \[hep-ph\]](#).
- [15] M. Knecht, H. Neufeld, H. Rupertsberger, and P. Talavera, “Chiral perturbation theory with virtual photons and leptons,” *Eur. Phys. J. C* **12** (2000) 469–478, [arXiv:hep-ph/9909284](#).
- [16] V. Cirigliano and I. Rosell, “ $\pi/K \rightarrow e \text{ anti-}\nu(e)$ branching ratios to $\mathcal{O}(e^{*2} p^{*4})$ in Chiral Perturbation Theory,” *JHEP* **10** (2007) 005, [arXiv:0707.4464 \[hep-ph\]](#).
- [17] J. Gasser and G. Zarnauskas, “On the pion decay constant,” *Phys. Lett. B* **693** (2010) 122–128, [arXiv:1008.3479 \[hep-ph\]](#).
- [18] V. Cirigliano and H. Neufeld, “A note on isospin violation in $\text{Pl}2(\gamma)$ decays,” *Phys. Lett. B* **700** (2011) 7–10, [arXiv:1102.0563 \[hep-ph\]](#).
- [19] V. Cirigliano, M. Knecht, H. Neufeld, H. Rupertsberger, and P. Talavera, “Radiative corrections to $K(13)$ decays,” *Eur. Phys. J. C* **23** (2002) 121–133, [arXiv:hep-ph/0110153 \[hep-ph\]](#).
- [20] V. Cirigliano, M. Giannotti, and H. Neufeld, “Electromagnetic effects in $K(13)$ decays,” *JHEP* **11** (2008) 006, [arXiv:0807.4507 \[hep-ph\]](#).

- [21] S. Descotes-Genon and B. Moussallam, “Radiative corrections in weak semi-leptonic processes at low energy: A Two-step matching determination,” *Eur. Phys. J. C* **42** (2005) 403–417, [arXiv:hep-ph/0505077](#).
- [22] N. Carrasco, V. Lubicz, G. Martinelli, C. T. Sachrajda, N. Tantalo, C. Tarantino, and M. Testa, “QED Corrections to Hadronic Processes in Lattice QCD,” *Phys. Rev.* **D91** no. 7, (2015) 074506, [arXiv:1502.00257 \[hep-lat\]](#).
- [23] M. G. Endres, A. Shindler, B. C. Tiburzi, and A. Walker-Loud, “Massive photons: an infrared regularization scheme for lattice QCD+QED,” *Phys. Rev. Lett.* **117** no. 7, (2016) 072002, [arXiv:1507.08916 \[hep-lat\]](#).
- [24] X. Feng and L. Jin, “QED self energies from lattice QCD without power-law finite-volume errors,” *Phys. Rev. D* **100** no. 9, (2019) 094509, [arXiv:1812.09817 \[hep-lat\]](#).
- [25] B. Lucini, A. Patella, A. Ramos, and N. Tantalo, “Charged hadrons in local finite-volume QED+QCD with C* boundary conditions,” *JHEP* **02** (2016) 076, [arXiv:1509.01636 \[hep-th\]](#).
- [26] V. Lubicz, G. Martinelli, C. T. Sachrajda, F. Sanfilippo, S. Simula, N. Tantalo, and C. Tarantino, “Electromagnetic corrections to the leptonic decay rates of charged pseudoscalar mesons: lattice results,” *PoS LATTICE2016* (2016) 290, [arXiv:1610.09668 \[hep-lat\]](#).
- [27] M. Di Carlo, D. Giusti, V. Lubicz, G. Martinelli, C. T. Sachrajda, F. Sanfilippo, S. Simula, and N. Tantalo, “Light-meson leptonic decay rates in lattice QCD+QED,” *Phys. Rev. D* **100** no. 3, (2019) 034514, [arXiv:1904.08731 \[hep-lat\]](#).
- [28] A. Desiderio *et al.*, “First lattice calculation of radiative leptonic decay rates of pseudoscalar mesons,” *Phys. Rev. D* **103** no. 1, (2021) 014502, [arXiv:2006.05358 \[hep-lat\]](#).
- [29] R. Frezzotti, N. Tantalo, G. Gagliardi, F. Sanfilippo, S. Simula, V. Lubicz, F. Mazzetti, G. Martinelli, and C. T. Sachrajda, “Lattice calculation of the Ds meson radiative form factors over the full kinematical range,” *Phys. Rev. D* **108** no. 7, (2023) 074505, [arXiv:2306.05904 \[hep-lat\]](#).
- [30] R. Frezzotti, G. Gagliardi, V. Lubicz, G. Martinelli, C. T. Sachrajda, F. Sanfilippo, S. Simula, and N. Tantalo, “The $B_s \rightarrow \mu^+ \mu^- \gamma$ decay rate at large q^2 from lattice QCD,” [arXiv:2402.03262 \[hep-lat\]](#).
- [31] M. Beneke, C. Bobeth, and R. Szafron, “Enhanced electromagnetic correction to the rare B-meson decay $B_{s,d} \rightarrow \mu^+ \mu^-$,” [arXiv:1708.09152 \[hep-ph\]](#).
- [32] M. Beneke, C. Bobeth, and R. Szafron, “Power-enhanced leading-logarithmic QED corrections to $B_q \rightarrow \mu^+ \mu^-$,” *JHEP* **10** (2019) 232, [arXiv:1908.07011 \[hep-ph\]](#).
- [33] C. Cornella, M. König, and M. Neubert, “Structure-dependent QED effects in exclusive B decays at subleading power,” *Phys. Rev. D* **108** no. 3, (2023) L031502, [arXiv:2212.14430 \[hep-ph\]](#).
- [34] M. Beneke, P. Böer, J.-N. Toelstede, and K. K. Vos, “Light-cone distribution amplitudes of light mesons with QED effects,” *JHEP* **11** (2021) 059, [arXiv:2108.05589 \[hep-ph\]](#).
- [35] M. Beneke, P. Böer, J.-N. Toelstede, and K. K. Vos, “Light-cone distribution amplitudes of heavy mesons with QED effects,” *JHEP* **08** (2022) 020, [arXiv:2204.09091 \[hep-ph\]](#).
- [36] E. Barberio, B. van Eijk, and Z. Was, “PHOTOS: A Universal Monte Carlo for QED radiative corrections in decays,” *Comput. Phys. Commun.* **66** (1991) 115–128.

- [37] E. Barberio and Z. Was, “PHOTOS: A Universal Monte Carlo for QED radiative corrections. Version 2.0,” *Comput. Phys. Commun.* **79** (1994) 291–308.
- [38] P. Golonka and Z. Was, “PHOTOS Monte Carlo: A Precision tool for QED corrections in Z and W decays,” *Eur. Phys. J. C* **45** (2006) 97–107, [arXiv:hep-ph/0506026](#).
- [39] N. Davidson, T. Przedzinski, and Z. Was, “PHOTOS interface in C++: Technical and Physics Documentation,” *Comput. Phys. Commun.* **199** (2016) 86–101, [arXiv:1011.0937 \[hep-ph\]](#).
- [40] M. Schonherr and F. Krauss, “Soft Photon Radiation in Particle Decays in SHERPA,” *JHEP* **12** (2008) 018, [arXiv:0810.5071 \[hep-ph\]](#).
- [41] **Sherpa** Collaboration, E. Bothmann *et al.*, “Event Generation with Sherpa 2.2,” *SciPost Phys.* **7** no. 3, (2019) 034, [arXiv:1905.09127 \[hep-ph\]](#).
- [42] T. Janowski, B. Pullin, and R. Zwicky, “Charged and neutral $\overline{B}_{u,d,s} \rightarrow \gamma$ form factors from light cone sum rules at NLO,” *JHEP* **12** (2021) 008, [arXiv:2106.13616 \[hep-ph\]](#).
- [43] G. P. Korchemsky, D. Pirjol, and T.-M. Yan, “Radiative leptonic decays of B mesons in QCD,” *Phys. Rev. D* **61** (2000) 114510, [arXiv:hep-ph/9911427](#).
- [44] E. Lunghi, D. Pirjol, and D. Wyler, “Factorization in leptonic radiative $B \rightarrow \gamma e \nu$ decays,” *Nucl. Phys. B* **649** (2003) 349–364, [arXiv:hep-ph/0210091](#).
- [45] S. Descotes-Genon and C. T. Sachrajda, “Factorization, the light cone distribution amplitude of the B meson and the radiative decay $B \rightarrow \gamma \ell \nu_\ell$,” *Nucl. Phys.* **B650** (2003) 356–390, [arXiv:hep-ph/0209216 \[hep-ph\]](#).
- [46] S. Bosch, R. Hill, B. Lange, and M. Neubert, “Factorization and Sudakov resummation in leptonic radiative B decay,” *Phys. Rev. D* **67** (2003) 094014, [arXiv:hep-ph/0301123](#).
- [47] M. Beneke and J. Rohrwild, “B meson distribution amplitude from $B \rightarrow \gamma \ell \nu$,” *Eur. Phys. J.* **C71** (2011) 1818, [arXiv:1110.3228 \[hep-ph\]](#).
- [48] V. Braun and A. Khodjamirian, “Soft contribution to $B \rightarrow \gamma \ell \nu_\ell$ and the B-meson distribution amplitude,” *Phys. Lett. B* **718** (2013) 1014–1019, [arXiv:1210.4453 \[hep-ph\]](#).
- [49] Y.-M. Wang, “Factorization and dispersion relations for radiative leptonic B decay,” *JHEP* **09** (2016) 159, [arXiv:1606.03080 \[hep-ph\]](#).
- [50] M. Beneke, V. Braun, Y. Ji, and Y.-B. Wei, “Radiative leptonic decay $B \rightarrow \gamma \ell \nu_\ell$ with subleading power corrections,” *JHEP* **07** (2018) 154, [arXiv:1804.04962 \[hep-ph\]](#).
- [51] Y.-L. Shen, Z.-T. Zou, and Y.-B. Wei, “Subleading power corrections to $B \rightarrow \gamma \ell \nu$ decay in PQCD approach,” *Phys. Rev. D* **99** no. 1, (2019) 016004, [arXiv:1811.08250 \[hep-ph\]](#).
- [52] Y.-M. Wang and Y.-L. Shen, “Subleading-power corrections to the radiative leptonic $B \rightarrow \gamma \ell \nu$ decay in QCD,” *JHEP* **05** (2018) 184, [arXiv:1803.06667 \[hep-ph\]](#).
- [53] F. Dettori, D. Guadagnoli, and M. Reboud, “ $B_s^0 \rightarrow \mu^+ \mu^- \gamma$ from $B_s^0 \rightarrow \mu^+ \mu^-$,” *Phys. Lett.* **B768** (2017) 163–167, [arXiv:1610.00629 \[hep-ph\]](#).
- [54] Y. G. Aditya, K. J. Healey, and A. A. Petrov, “Faking $B_s \rightarrow \mu^+ \mu^-$,” *Phys. Rev.* **D87** (2013) 074028, [arXiv:1212.4166 \[hep-ph\]](#).
- [55] D. Guadagnoli, M. Reboud, and R. Zwicky, “Bs to l+ l- gamma as a Test of Lepton Flavor Universality,” [arXiv:1708.02649 \[hep-ph\]](#).

- [56] A. Kozachuk, D. Melikhov, and N. Nikitin, “Rare FCNC radiative leptonic $B_{s,d} \rightarrow \gamma l^+ l^-$ decays in the standard model,” *Phys. Rev.* **D97** no. 5, (2018) 053007, [arXiv:1712.07926 \[hep-ph\]](#).
- [57] M. Beneke, C. Bobeth, and Y.-M. Wang, “ $B_{d,s} \rightarrow \gamma \ell \bar{\ell}$ decay with an energetic photon,” [arXiv:2008.12494 \[hep-ph\]](#).
- [58] A. Carvunis, F. Dettori, S. Gangal, D. Guadagnoli, and C. Normand, “On the effective lifetime of $B_s \rightarrow \mu\mu\gamma$,” [arXiv:2102.13390 \[hep-ph\]](#).
- [59] D. Melikhov and N. Nikitin, “Rare radiative leptonic decays $B(d,s) \rightarrow l^+ l^- \gamma$,” *Phys. Rev.* **D70** (2004) 114028, [arXiv:hep-ph/0410146 \[hep-ph\]](#).
- [60] B. Pullin and R. Zwicky, “Radiative Decays of Heavy-light Mesons and the $f_{H,H^*,H_1}^{(T)}$ Decay Constants,” [arXiv:2106.13617 \[hep-ph\]](#).
- [61] R. E. Cutkosky, “Singularities and discontinuities of Feynman amplitudes,” *J. Math. Phys.* **1** (1960) 429–433.
- [62] B. W. Harris and J. Smith, “Heavy quark correlations in deep inelastic electroproduction,” *Nucl. Phys. B* **452** (1995) 109–160, [arXiv:hep-ph/9503484](#).
- [63] W. Beenakker, H. Kuijf, W. L. van Neerven, and J. Smith, “QCD Corrections to Heavy Quark Production in p anti-p Collisions,” *Phys. Rev.* **D40** (1989) 54–82.
- [64] G. Somogyi, “Angular integrals in d dimensions,” *J. Math. Phys.* **52** (2011) 083501, [arXiv:1101.3557 \[hep-ph\]](#).
- [65] S. Borowka, G. Heinrich, S. Jahn, S. P. Jones, M. Kerner, J. Schlenk, and T. Zirke, “pySecDec: a toolbox for the numerical evaluation of multi-scale integrals,” *Comput. Phys. Commun.* **222** (2018) 313–326, [arXiv:1703.09692 \[hep-ph\]](#).
- [66] B. W. Harris and J. F. Owens, “The Two cutoff phase space slicing method,” *Phys. Rev.* **D65** (2002) 094032, [arXiv:hep-ph/0102128 \[hep-ph\]](#).
- [67] G. F. Sterman, *An Introduction to quantum field theory*. Cambridge University Press, 8, 1993.
- [68] A. Sirlin, “Large $m(W)$, $m(Z)$ Behavior of the $O(\alpha)$ Corrections to Semileptonic Processes Mediated by W,” *Nucl. Phys. B* **196** (1982) 83–92.
- [69] J. Brod and M. Gorbahn, “Electroweak Corrections to the Charm Quark Contribution to $K^+ \rightarrow \pi^+ \nu \text{ anti-}\nu$,” *Phys. Rev. D* **78** (2008) 034006, [arXiv:0805.4119 \[hep-ph\]](#).
- [70] M. Gorbahn, S. Jäger, F. Moretti, and E. van der Merwe, “Semileptonic weak Hamiltonian to $\mathcal{O}(\alpha_s)$ in momentum-space subtraction schemes,” *JHEP* **01** (2023) 159, [arXiv:2209.05289 \[hep-ph\]](#).
- [71] D. Bigi, M. Bordone, P. Gambino, U. Haisch, and A. Piccione, “QED effects in inclusive semi-leptonic B decays,” *JHEP* **11** (2023) 163, [arXiv:2309.02849 \[hep-ph\]](#).
- [72] M. A. Shifman, “Quark hadron duality,” in *8th International Symposium on Heavy Flavor Physics*, vol. 3, pp. 1447–1494. World Scientific, Singapore, 7, 2000. [arXiv:hep-ph/0009131](#).
- [73] M. A. Shifman, A. I. Vainshtein, and V. I. Zakharov, “QCD and Resonance Physics. Theoretical Foundations,” *Nucl. Phys. B* **147** (1979) 385–447.
- [74] M. A. Shifman, A. I. Vainshtein, and V. I. Zakharov, “QCD and Resonance Physics: Applications,” *Nucl. Phys. B* **147** (1979) 448–518.

- [75] P. Ball and R. Zwicky, “New results on $B \rightarrow \pi, K, \eta$ decay formfactors from light-cone sum rules,” *Phys. Rev. D* **71** (2005) 014015, [arXiv:hep-ph/0406232](#).
- [76] I. I. Y. Bigi, M. A. Shifman, N. G. Uraltsev, and A. I. Vainshtein, “The Pole mass of the heavy quark. Perturbation theory and beyond,” *Phys. Rev. D* **50** (1994) 2234–2246, [arXiv:hep-ph/9402360](#).
- [77] M. Rowe and R. Zwicky, “Isospin mass differences of the B, D and K,” *JHEP* **06** (2023) 089, [arXiv:2301.04972 \[hep-ph\]](#).
- [78] P. Gambino, A. Melis, and S. Simula, “Extraction of heavy-quark-expansion parameters from unquenched lattice data on pseudoscalar and vector heavy-light meson masses,” *Phys. Rev. D* **96** no. 1, (2017) 014511, [arXiv:1704.06105 \[hep-lat\]](#).
- [79] D. Becirevic, B. Haas, and E. Kou, “Soft Photon Problem in Leptonic B-decays,” *Phys. Lett. B* **681** (2009) 257–263, [arXiv:0907.1845 \[hep-ph\]](#).
- [80] **Belle-II** Collaboration, W. Altmannshofer *et al.*, “The Belle II Physics Book,” *PTEP* **2019** no. 12, (2019) 123C01, [arXiv:1808.10567 \[hep-ex\]](#). [Erratum: PTEP 2020, 029201 (2020)].
- [81] **Flavour Lattice Averaging Group (FLAG)** Collaboration, Y. Aoki *et al.*, “FLAG Review 2021,” *Eur. Phys. J. C* **82** no. 10, (2022) 869, [arXiv:2111.09849 \[hep-lat\]](#).
- [82] G. Ricciardi, “Theory: Semileptonic B Decays and $|V_{xb}|$ update,” *PoS BEAUTY2020* (2021) 031, [arXiv:2103.06099 \[hep-ph\]](#).
- [83] **Belle** Collaboration, I. Adachi *et al.*, “Evidence for $B^- \rightarrow \tau^- \bar{\nu}_\tau$ with a Hadronic Tagging Method Using the Full Data Sample of Belle,” *Phys. Rev. Lett.* **110** no. 13, (2013) 131801, [arXiv:1208.4678 \[hep-ex\]](#).
- [84] **Belle** Collaboration, B. Kronenbitter *et al.*, “Measurement of the branching fraction of $B^+ \rightarrow \tau^+ \nu_\tau$ decays with the semileptonic tagging method,” *Phys. Rev. D* **92** no. 5, (2015) 051102, [arXiv:1503.05613 \[hep-ex\]](#).
- [85] **BaBar** Collaboration, B. Aubert *et al.*, “A Search for $B^+ \rightarrow \ell^+ \nu_\ell$ Recoiling Against $B^- \rightarrow D^0 \ell^- \bar{\nu} X$,” *Phys. Rev. D* **81** (2010) 051101, [arXiv:0912.2453 \[hep-ex\]](#).
- [86] **BaBar** Collaboration, J. P. Lees *et al.*, “Measurement of an Excess of $\bar{B} \rightarrow D^{(*)} \tau^- \bar{\nu}_\tau$ Decays and Implications for Charged Higgs Bosons,” *Phys. Rev. D* **88** no. 7, (2013) 072012, [arXiv:1303.0571 \[hep-ex\]](#).
- [87] **Particle Data Group** Collaboration, P. A. Zyla *et al.*, “Review of Particle Physics,” *PTEP* **2020** no. 8, (2020) 083C01.
- [88] M. Tanaka and R. Watanabe, “New physics contributions in $B \rightarrow \pi \tau \bar{\nu}$ and $B \rightarrow \tau \bar{\nu}$,” *PTEP* **2017** no. 1, (2017) 013B05, [arXiv:1608.05207 \[hep-ph\]](#).
- [89] R. Mertig, M. Bohm, and A. Denner, “FEYN CALC: Computer algebraic calculation of Feynman amplitudes,” *Comput. Phys. Commun.* **64** (1991) 345–359.
- [90] V. Shtabovenko, R. Mertig, and F. Orellana, “FeynCalc 9.3: New features and improvements,” *Comput. Phys. Commun.* **256** (2020) 107478, [arXiv:2001.04407 \[hep-ph\]](#).
- [91] H. H. Patel, “Package-X 2.0: A Mathematica package for the analytic calculation of one-loop integrals,” *Comput. Phys. Commun.* **218** (2017) 66–70, [arXiv:1612.00009 \[hep-ph\]](#).
- [92] G. S. Bali, F. Bruckmann, M. Constantinou, M. Costa, G. Endrodi, S. D. Katz, H. Panagopoulos, and A. Schafer, “Magnetic susceptibility of QCD at zero and at finite

temperature from the lattice,” *Phys. Rev. D* **86** (2012) 094512, [arXiv:1209.6015](#) [[hep-lat](#)].

- [93] Z.-G. Wang, “Analysis of heavy mesons in nuclear matter with a QCD sum rule approach,” *Phys. Rev. C* **92** no. 6, (2015) 065205, [arXiv:1501.05093](#) [[hep-ph](#)].